

# The Abundance Properties of Nearby Late-Type Galaxies.

## I. The Data

L. S. Pilyugin<sup>1</sup> and E. K. Grebel

Astronomisches Rechen-Institut, Zentrum für Astronomie der Universität Heidelberg,  
Mönchhofstr. 12–14, 69120 Heidelberg, Germany

pilyugin@mao.kiev.ua, grebel@ari.uni-heidelberg.de

A. Y. Kniazev<sup>2,3</sup>

South African Astronomical Observatory, PO Box 9, 7935 Observatory, Cape Town, South  
Africa

akniazev@sao.ac.za

Received \_\_\_\_\_; accepted \_\_\_\_\_

---

<sup>1</sup>Visiting Astronomer, Main Astronomical Observatory of National Academy of Sciences of Ukraine, 27 Zabolotnogo str., 03680 Kiev, Ukraine.

<sup>2</sup>Southern African Large Telescope Foundation, PO Box 9, 7935 Observatory, Cape Town, South Africa.

<sup>3</sup>Sternberg Astronomical Institute, Lomonosov Moscow State University, Moscow 119992, Russia

## ABSTRACT

We investigate the oxygen and nitrogen abundance distributions across the optical disks of 130 nearby late-type galaxies using around 3740 published spectra of H II regions. We use these data in order to provide homogeneous abundance determinations for all objects in the sample, including H II regions in which not all of the usual diagnostic lines were measured. Examining the relation between N and O abundances in these galaxies we find that the abundances in their centres and at their isophotal  $R_{25}$  disk radii follow the same relation. The variation in N/H at a given O/H is around 0.3 dex. We suggest that the observed spread in N/H may be partly caused by the time delay between N and O enrichment and the different star formation histories in galaxies of different morphological types and dimensions. We study the correlations between the abundance properties (central O and N abundances, radial O and N gradients) of a galaxy and its morphological type and dimension.

*Subject headings:* galaxies: abundances – galaxies: ISM – galaxies: spiral – galaxies:irregular

## 1. Introduction

The chemical composition of a galaxy is one of its most fundamental characteristics. Here we focus on disk galaxies. Because the chemical enrichment depends on various physical processes, such as the star formation history and the mass exchange between the galaxy and its environment, progress in our understanding of galaxy formation and evolution processes depends to a large extent on improving our knowledge of the detailed chemical properties of galaxies, such as the radial distribution of element abundances across galactic disks. Establishing the macroscopic properties of spiral and irregular galaxies that likely govern the distribution of heavy elements across their disks is very important in understanding the (chemical) evolution of galaxies.

Accurate abundance determinations in a sample of galaxies are mandatory for such investigations. The classical  $T_e$  method, often referred to as the direct method, is generally considered to provide the most reliable oxygen and nitrogen abundances in H II regions. When this method cannot be used (due to the lack of measurements of the required weak auroral lines in the spectra of H II regions) then combinations of the strong nebular line intensities in spectra of H II regions can be used as indicators of their oxygen abundances, as was first suggested by Pagel et al. (1979) and Alloin et al. (1979). This approach is usually referred to as the “strong-line method” and has been widely adopted. The establishment of calibrations (i.e., of relations between metallicity-sensitive emission-line combinations and metallicity) was the subject of numerous studies (Dopita & Evans 1986; McGaugh 1991; Pilyugin 2000, 2001; Kewley & Dopita 2002; Pettini & Pagel 2004; Tremonti et al. 2004; Liang et al. 2006; Stasińska 2006; Thuan et al. 2010, among many others).

A calibration is defined not only by the adopted indicators but also by the objects that serve as calibrating data points. A sample of H II regions with abundances derived through the  $T_e$  method is used to construct an empirical calibration. A set of photoionization

models is used to construct a theoretical (model) calibration. Even if the same indicator is used in the empirical calibration and in the theoretical calibration and if the same spectral measurements in a given H II region are used, those calibrations can produce significantly different abundance estimations. Metallicities derived using theoretical calibrations tend to be systematically higher (up to  $\sim 0.7$  dex) than those derived using the empirical calibrations (see reviews by Kewley & Ellison 2008; López-Sánchez & Esteban 2010; López-Sánchez et al. 2012). Therefore, oxygen abundances in extragalactic H II regions obtained in different studies using different calibrations can be significantly different.

Spectroscopic measurements of H II regions within and beyond optical radii of galaxies were carried out in many works (see list of references below). In these studies, usually the H II regions in one or several galaxies are measured and the radial distributions of the element abundances across the disks of those galaxies are estimated. Since often different methods for abundance determinations are used in different works, the resulting abundances from these studies are not homogeneous and cannot be directly compared to each other. Therefore, the abundances in a sample of galaxies can be analyzed only after those abundances are homogenized, i.e., all the abundances are redetermined in a uniform way. This is the first step in our present investigation. It should be noted that there have been several attempts to use uniform abundances for the determination of radial abundance gradients in a sample of galaxies; e.g., Vila-Costas & Edmunds (1992) for a sample of 30 galaxies, Zaritsky et al. (1994) for 39 galaxies, van Zee et al. (1998) for 11 galaxies, Pilyugin et al. (2004) for 54 galaxies, and Moustakas et al. (2010) for 21 galaxies. However, those samples contain a relatively small number of galaxies (whereas our present sample includes 130 galaxies).

So far, little attention has been paid to the radial distributions of nitrogen abundances in the disks of galaxies, despite the fact that this provides several advantages for the study

of the chemical evolution of galaxies. Indeed, since at  $12+\log(\text{O}/\text{H}) \gtrsim 8.3$ , secondary nitrogen becomes dominant and the nitrogen abundance increases at a faster rate than the oxygen abundance (e.g., Henry et al. 2000), the change in nitrogen abundances with galactocentric distance should then show a larger amplitude in comparison to oxygen abundances and, as a consequence, should be easier to measure. Furthermore, there is a time delay in nitrogen production as compared to oxygen production (Maeder 1992; van den Hoek & Groenewegen 1997; Pagel 1997). Thus the comparison between the radial distributions of oxygen and nitrogen abundances in the disks of galaxies can shed additional light on the chemical evolution of galaxies. Therefore we consider here not only the radial distributions of oxygen abundances but also those of nitrogen abundances.

Our paper is organized in the following way. We describe the method used for the oxygen and nitrogen abundance determinations in the H II regions of our galaxy sample in Section 2. We describe the observational data that were used to determine the abundances in the H II regions in Section 3. We discuss the abundance properties in the disks of nearby galaxies (within the optical isophotal radii) in Section 4. We summarize our results in Section 5.

Throughout this paper, we will use the following standard notations for the line intensities:

$$R_2 = I_{[\text{O II}]\lambda 3727+\lambda 3729}/I_{\text{H}\beta},$$

$$N_2 = I_{[\text{N II}]\lambda 6548+\lambda 6584}/I_{\text{H}\beta},$$

$$S_2 = I_{[\text{S II}]\lambda 6717+\lambda 6731}/I_{\text{H}\beta},$$

$$R_3 = I_{[\text{O III}]\lambda 4959+\lambda 5007}/I_{\text{H}\beta}.$$

With these definitions, the excitation parameter  $P$  can be expressed as:  $P = R_3/(R_2+R_3)$ .

## 2. Abundance determination

### 2.1. Modification of the $C$ method

A new method (called the “ $C$  method”) for oxygen and nitrogen abundance determinations has recently been suggested (Pilyugin et al. 2012). The idea of the  $C$  method is a very simple. We have compared a several combinations of the strong-line intensities in the spectrum of a given H II region with those in the spectra of a sample of reference H II regions with known abundances in order to find the counterpart for the H II region under study. It is assumed that the oxygen and nitrogen abundances in the studied H II region are the same as in its counterpart. A counterpart can be selected by comparison of four combinations of strong-line intensities:  $P = R_3/(R_2 + R_3)$  (excitation parameter),  $\log R_3$ ,  $\log(N_2/R_2)$ , and  $\log(S_2/R_2)$ .

However, there are recent measurements of spectra of many H II regions where the intensities of [O II] $\lambda 3727 + \lambda 3729$  or [S II] $\lambda 6717$ , [S II] $\lambda 6731$  lines are not available (e.g., in Sánchez et al. (2012) or in the Sloan Digital Sky Survey (SDSS); see York et al. (2000)). It has been argued that the oxygen and nitrogen abundances in H II regions can be estimated even if the [S II] $\lambda 6717 + \lambda 6731$  emission line is not measured (Pilyugin et al. 2010) or if the [O II] $\lambda 3727 + \lambda 3729$  emission line is not available (Pilyugin & Mattsson 2011). The  $C$  method can be adapted to such cases (Pilyugin et al. 2013). To find the counterpart for the H II region under study, one does not need to compare the four combinations of strong-line intensities, but can instead also use only three combinations: 1)  $\log R_3$ ,  $P$ , and  $\log(N_2/R_2)$ , or 2)  $\log R_3$ ,  $\log N_2$ , and  $\log(N_2/S_2)$ . When this first set of combinations of strong-line intensities is used to find the counterpart then the resulting oxygen and nitrogen abundances will be referred to as  $(O/H)_{C_{ON}}$  and  $(N/H)_{C_{ON}}$ . When the second set of combinations of strong-line intensities is used to find the counterpart then the inferred oxygen and nitrogen abundances will be called  $(O/H)_{C_{NS}}$  and  $(N/H)_{C_{NS}}$ .

The data for reference H II regions with  $T_e$ -based abundances are compiled in Pilyugin et al. (2012). The very recent spectroscopic observations of Berg et al. (2012); Zurita & Bresolin (2012); Skillman et al. (2013) have been added to the compilation. Using these combined data we select a sample of reference H II regions for which all the absolute differences for oxygen abundances  $(\text{O}/\text{H})_{C_{\text{ON}}} - (\text{O}/\text{H})_{T_e}$  and  $(\text{O}/\text{H})_{C_{\text{NS}}} - (\text{O}/\text{H})_{T_e}$  and for nitrogen abundances  $(\text{N}/\text{H})_{C_{\text{ON}}} - (\text{N}/\text{H})_{T_e}$  and  $(\text{N}/\text{H})_{C_{\text{NS}}} - (\text{N}/\text{H})_{T_e}$  are less than 0.1 dex. This sample of reference H II regions contains 250 objects and will in the following be used for abundance determinations. This sample will be referred to as *E2013* sample (etalon sample 2013) below.

## 2.2. Modification of the $P$ method

Furthermore, only blue spectra were observed for H II regions in a number of galaxies (e.g., Oey & Kennicutt 1993; Zaritsky et al. 1994; Werk et al. 2011), i.e., intensities of [N II] $\lambda$ 6584 and [S II] $\lambda$ 6717, [S II] $\lambda$ 6731) are not available in those cases. The oxygen abundances in those H II regions can be estimated through the  $P$  calibration where only the oxygen [O II] $\lambda$ 3727+ $\lambda$ 3729 and [O III] $\lambda$ 5007 lines are used (Pilyugin 2000, 2001; Pilyugin & Thuan 2005). We have constructed a new variant of the  $P$  calibration. The sample of reference H II regions, *E2013*, has been used as calibration data points. To enlarge the number of calibration data points, we have added a number of H II regions with  $(\text{O}/\text{H})_{C_{\text{ON}}}$  abundances that were chosen in the following way. We determined the  $(\text{O}/\text{H})_{C_{\text{ON}}}$  abundances in H II regions and obtained radial oxygen abundance gradients across the disks of galaxies (see below). The H II regions where the deviations of the  $(\text{O}/\text{H})_{C_{\text{ON}}}$  abundances from the general radial abundance trend are less than 0.1 dex were added to the sample of reference H II regions.

It is well known that the relation between the oxygen abundance and the strong oxygen

line intensities is double-valued, with two distinct parts traditionally known as the upper and lower branches of the  $R_{23} - O/H$  diagram. We have delimited the upper and lower branches and the transition zone, adopting  $12 + \log(O/H) = 8.3$  as the boundary between the upper branch and the transition zone and  $12 + \log(O/H) = 8.0$  as the boundary between the transition zone and the lower branch. These boundaries are somewhat arbitrary, but were chosen so as to give the best calibrations with the existing data. Two distinct relations between the oxygen abundance and the strong oxygen line intensities will be established in the following, one for the upper branch (the high-metallicity calibration) and one for the lower branch (the low-metallicity calibration).

The relation between the oxygen abundance  $Z_P \equiv 12 + \log(O/H)_P$  and  $R_3$  and  $P$  can be fitted by a polynomial of the form (Pilyugin 2001; Pilyugin & Thuan 2005)

$$Z_P = k_0 + k_1 \log R_3 + k_2 (\log R_3)^2, \quad (1)$$

where we have used the notation  $Z \equiv 12 + \log(O/H)$  for brevity. To take into account the dependence on the excitation parameter  $P$ , the coefficients of Eq. (1) are chosen to have the form

$$k_j = a_j + b_j P. \quad (2)$$

The coefficients  $a_0$ ,  $a_1$ ,  $a_2$ ,  $b_0$ ,  $b_1$ , and  $b_2$  can then be determined by looking for the best fit to our sample of H II regions. We wish to derive a set of coefficients in Eq. (1) which gives the minimum value of  $\langle \Delta(O/H) \rangle = \sqrt{(\sum_{j=1}^n (\Delta(O/H)_j)^2)/n}$ . Here  $\Delta(O/H)_j$  is equal to  $\log(O/H)_{P,j} - \log(O/H)_{T_e, C_{ON},j}$  for each H II region in our sample. The quantity  $\langle \Delta(O/H) \rangle$  is the average value of the differences between the oxygen abundances determined through the  $P$  calibration and the original ones. A few data points with large deviations, in excess of 0.15 dex, are rejected, and are not used in the determination of the final relation.



The obtained upper-branch  $P$  calibration (for  $12 + \log(\text{O}/\text{H}) \gtrsim 8.3$ ) is

$$\begin{aligned} Z_P &= 8.334 + 0.533 P \\ &- (0.338 + 0.415 P) \log R_3 \\ &- (0.086 - 0.225 P) (\log R_3)^2 \end{aligned} \tag{3}$$

The obtained lower-branch  $P$  calibration (for  $12 + \log(\text{O}/\text{H}) \lesssim 8.0$ ) is

$$\begin{aligned} Z_P &= 7.949 - 1.328 P \\ &+ (0.926 - 0.440 P) \log R_3 \\ &+ (1.220 - 0.480 P) (\log R_3)^2 \end{aligned} \tag{4}$$

Hence, here we use the empirical metallicity scale defined by the H II regions with abundances derived through the direct method ( $T_e$  method).

### 3. The data

We have carried out a fairly comprehensive compilation of published spectra of H II regions in late-type galaxies. Only those galaxies where radial abundance gradients can be estimated were taken into consideration.

#### 3.1. The general properties of our sample of galaxies

Our final list includes 130 galaxies. Table 1 lists the general characteristics of each galaxy. The first column gives its name. We have used the most widely used name for each galaxy. The galaxies are listed in order of name category, with the following categories in descending order:

NGC – New General Catalogue,

IC – Index Catalogue,

UGC – Uppsala General Catalog of Galaxies,

PGC – Catalogue of Principal Galaxies.

The morphological type of the galaxy and morphological type code  $T$  from LEDA are reported in columns 2 and 3. The right ascension (R.A.) and declination (Decl.) (J2000.0) of each galaxy are given in columns 4 and 5. The right ascension and declination are taken from the NASA/IPAC Extragalactic Database (NED)<sup>1</sup>. The isophotal radius  $R_{25}$  in arcmin of each galaxy is reported in column 6. Unless otherwise stated, the  $R_{25}$  values are taken from de Vaucouleurs et al. (1991, thereafter RC3). The position angle and inclination are listed in columns 7 and 8, and the sources for these values are given in column 9. The adopted distance and its reference are reported in columns 10 and 11. The NED distances use flow corrections for Virgo, the Great Attractor, and Shapley Supercluster infall. The isophotal radius in kpc, estimated from the data in columns 6 and 10, is listed in column 12.

### 3.2. A compilation of the line intensities in spectra of H II regions

We have carried out an extensive search of the literature and compiled a sample of measurements of H II regions in nearby late-type galaxies. We have searched for spectra of H II regions with the requirement that they include the [O II] $\lambda$ 3727+ $\lambda$ 3729, [O III] $\lambda$ 5007, [N II] $\lambda$ 6584, and [S II] $\lambda$ 6717+ $\lambda$ 6731 lines. While we have tried to include as many sources as possible, we do not claim our search to be exhaustive.

Thus, for each listed spectrum, we record the measured values of [O II] $\lambda$ 3727+ $\lambda$ 3729, [O III] $\lambda$ 5007, [N II] $\lambda$ 6584, [S II] $\lambda$ 6717, and [S II] $\lambda$ 6731. The intensities of all lines are

---

<sup>1</sup>The NASA/IPAC Extragalactic Database (NED) is operated by the Jet Propulsion Laboratory, California Institute of Technology, under contract with the National Aeronautics and Space Administration. <http://ned.ipac.caltech.edu/>

normalised to the  $H\beta$  line flux. The predicted values of the flux ratio of oxygen  $[O\text{ III}]\lambda 5007/[O\text{ III}]\lambda 4959$  and nitrogen  $[N\text{ II}]\lambda 6584/[N\text{ II}]\lambda 6548$  lines are very close to three (Storey & Zeppen 2000). The measurements of the  $[O\text{ III}]\lambda 5007$  and  $\lambda 4959$  lines in SDSS spectra confirm this value of the flux ratio (e.g., Kniazev et al. 2004). Therefore, the value of  $R_3$  can be estimated without  $[O\text{ III}]\lambda 4959$  line as  $R_3 = 1.33[O\text{ III}]\lambda 5007$ , and, similarly, the values of  $N_2$  are estimated without the lines  $[N\text{ II}]\lambda 6548$  as  $N_2 = 1.33[N\text{ II}]\lambda 6584$ .

We have taken the de-reddened line intensities as reported by the authors. In some papers only the measured fluxes are reported. In these cases, the measured emission-line fluxes were corrected for interstellar reddening using the theoretical  $H\alpha$  to  $H\beta$  ratio (i.e., the standard value of  $H\alpha/H\beta = 2.86$ ) and the analytical approximation to the Whitford interstellar reddening law from Izotov et al. (1994).

The spectroscopic data so assembled form the basis of the present study. Our total list contains 3904 spectra including 162 spectra of H II regions beyond the isophotal radius  $R_{25}$ . Here we will examine the radial oxygen and nitrogen abundance distributions within the isophotal radius in every galaxy. The radial oxygen and nitrogen abundances beyond the isophotal radius will be discussed elsewhere.

## 4. Abundances

### 4.1. Radial abundance gradients

When measurements of the lines  $[O\text{ II}]\lambda 3727+\lambda 3729$ ,  $[O\text{ III}]\lambda 5007$ , and  $[N\text{ II}]\lambda 6584$  were available then the oxygen  $(O/H)_{\text{CON}}$  and nitrogen  $(N/H)_{\text{CON}}$  abundances in the H II regions were estimated and used in our study. If the intensity of the line  $[O\text{ II}]\lambda 3727+\lambda 3729$  was not measured but the measurements of the lines  $[O\text{ III}]\lambda 5007$ ,  $[N\text{ II}]\lambda 6584$ ,  $[S\text{ II}]\lambda 6717$ , and  $[S\text{ II}]\lambda 6731$  were available then the oxygen  $(O/H)_{\text{CNS}}$  and nitrogen  $(N/H)_{\text{CNS}}$  abundances

of the H II regions were estimated and used. If the measurements of only the oxygen lines [O II] $\lambda$ 3727+ $\lambda$ 3729 and [O III] $\lambda$ 5007 were available (blue spectrum was observed only) then the oxygen (O/H)<sub>P</sub> abundance of the H II regions was estimated and adopted.

The deprojected radii of the H II regions were computed using their coordinates (or offsets from the nucleus) as reported in the original papers, as were the position angle and inclination listed in Table 1. In some publications, the positions of the observed H II regions (or their identifications in catalogues) were not reported, but the deprojected radii were listed instead. In these cases these deprojected radii were used (after correction for the galaxy distance adopted here, if necessary). The fractional radii (normalized to the optical isophotal radius  $R_{25}$ ) were obtained with isophotal radii from Table 1.

The radial oxygen abundance distribution within the isophotal radius in every galaxy was fitted by the following equation:

$$12 + \log(\text{O/H}) = 12 + \log(\text{O/H})_{R_0} + C_{\text{O/H}} \times (R/R_{25}), \quad (5)$$

where  $12 + \log(\text{O/H})_{R_0}$  is the oxygen abundance at  $R_0 = 0$ , i.e., the extrapolated central oxygen abundance,  $C_{\text{O/H}}$ , is the slope of the oxygen abundance gradient expressed in terms of dex  $R_{25}^{-1}$ , and  $R/R_{25}$  is the fractional radius (the galactocentric distance normalized to the disk’s isophotal radius  $R_{25}$ ). We also determined the oxygen abundance gradient expressed in terms of dex kpc<sup>−1</sup>. If there were data points with large deviations, in excess of 0.2 dex, those points were rejected, and were not used in the determination of the final relation.

The derived parameters of the oxygen abundance distributions are presented in Table 2. The name of the galaxy is listed in column 1. The extrapolated central  $12 + \log(\text{O/H})_{R_0}$  oxygen abundance and the gradient (the coefficient  $C_{\text{O/H}}$  in Eq. (5)) expressed in terms of dex  $R_{25}^{-1}$  are listed in columns 2 and 3. The oxygen abundance gradient expressed in terms of dex kpc<sup>−1</sup> is listed in column 4. The scatter of oxygen abundances around the general

radial oxygen abundance trend is reported in column 5.

As in the case of the oxygen abundance, the radial nitrogen abundance distribution in every galaxy was fitted by the following equation:

$$12 + \log(\text{N}/\text{H}) = 12 + \log(\text{N}/\text{H})_{R_0} + C_{\text{N}/\text{H}} \times (R/R_{25}). \quad (6)$$

Again, if there were data points with large deviations, in excess of 0.3 dex, those points were rejected, and were not used in the determination of the final relation. These different rejection criteria for oxygen abundances, 0.2 dex, and nitrogen abundances, 0.3 dex, are used for the following reason. There is no one-to-one correspondence between nitrogen and oxygen abundances, but instead there is a scatter in N/H at a given O/H. Therefore one can expect that the natural scatter in N/H at a given galactocentric distance can be larger than that in O/H assuming similar uncertainties in both abundance determinations. The derived parameters of the nitrogen abundance distributions are presented in Table 2. The extrapolated central  $12 + \log(\text{N}/\text{H})_{R_0}$  nitrogen abundance and the gradient (the coefficient  $C_{\text{N}/\text{H}}$  in Eq. (6)) expressed in terms of dex  $R_{25}^{-1}$  are listed in columns 6 and 7. The nitrogen abundance gradient expressed in terms of dex  $\text{kpc}^{-1}$  is listed in column 8. The scatter of nitrogen abundances around the general radial nitrogen abundance trend is reported in column 9.

A list of references for the emission line flux measurements in the H II regions is given in Table 3.

In the case of  $(\text{O}/\text{H})_P$  abundances, there is the following problem. The relationship between oxygen abundance and strong oxygen line intensities, the  $P$  calibration, is double-valued with two distinct parts usually known as the “lower” and “upper” branches of the  $R_{23} - \text{O}/\text{H}$  relationship. The expression for the oxygen abundance determination in high metallicity H II regions, Eq. (3), is valid only for H II regions that belong to the upper branch, with  $12 + \log(\text{O}/\text{H}) \gtrsim 8.3$ . Thus, one has to know a priori on which of the

two branches the H II region lies. We can overcome this problem in the way suggested in Pilyugin et al. (2004). It has been known for a long time (Searle 1971; Smith 1975) that disks of spiral galaxies show radial oxygen abundance gradients, in the sense that the oxygen abundance is higher in the central part of the disk and decreases with galactocentric distance. We thus start from the H II regions in the central part of disks and move outward until the radius  $R^*$  where the oxygen abundance decreases to  $12+\log(\text{O}/\text{H}) \sim 8.3$ . It should be noted that it is difficult to establish the exact value of  $R^*$  due to the scatter in oxygen abundance values at any fixed radius. An unjustified use of Eq. (3) in the determination of the oxygen abundance in low-metallicity H II regions beyond  $R^*$  would result in overestimated oxygen abundances, and would produce a false turnover in the slope of the abundance gradients (Pilyugin 2003). Therefore, H II regions with galactocentric distances larger than  $R^*$ , i.e., those with  $12+\log(\text{O}/\text{H}) \lesssim 8.3$  were rejected.

The derived radial distributions of the oxygen and nitrogen abundances in 130 galaxies are presented in Figure 1. The oxygen abundances for individual H II regions are indicated by points. All the data points (including points with large deviations, which are rejected and are not used in determination of the final relation) are shown. The linear best fits (derived via the least squares method) to the points are represented by solid lines. The galactocentric distances are normalized to the isophotal radius. The nitrogen abundances for individual H II regions are shown by the plus signs. The linear best fits to the points are indicated by dashed lines.

The values of the gradients in a number of galaxies (e.g., in NGC 12, the first galaxy in our list) are rather small and are comparable (or even lower) to the uncertainties of gradients. It can be assumed that there is no abundance gradient in such a galaxy, and its abundance can be specified by the mean of the central abundance and the abundance at the isophotal  $R_{25}$  radius of the galaxy.

Thus, the radial oxygen and nitrogen abundance distributions across the optical disk in every galaxy are individually fitted by a single relation. It looks like a rather good approximation for the majority of galaxies. However, a small change in slope in the abundance distribution cannot be excluded in the disks of several galaxies (e.g., NGC 925, NGC 3184, NGC 5457). It is interesting to note the following. Pohlen & Trujillo (2006) studied the surface brightness profiles of a sample of late-type (Sb to Sdm) spiral galaxies using imaging data from the SDSS survey. They found that the surface brightness profiles can be divided into three classes. A small fraction of galaxies (around 10 %) belong to type I, which comprises those galaxies that have a normal (standard) exponential disk down to the noise limit. The surface brightness distribution of the rest of the galaxies is better described as a broken exponential. About 60 % of the galaxies belong to type II, which means that they show a down-bending profile with steeper outer part. About 30 % of the galaxies belong to type III, implying that they show an up-bending profile with shallower outer part. Thus, the abundance distribution profile does not seem to follow strictly the slope of the surface brightness profile. It should be noted, however, that the number of measured H II regions in many galaxies is too small to allow one to detect a small bend in the radial abundance distribution.

#### 4.2. Notes on individual galaxies

**NGC 1512.** The five H II regions that are located in the “bridge” between the interacting galaxies NGC 1512 and NGC 1510 (Bresolin et al. 2012) were excluded from our analysis. Dicaire et al. (2008) found that there is a significant discrepancy between the kinematically derived inclination of NGC 1512 and its photometric value ( $i_{phot} = 65^\circ$  and  $i_{kin} = 35^\circ$ ). They noted that the explanation is quite clear: the photometric parameter is mainly representative of the bar which contributes a large part of the light resulting in

more edge-on values. However, the outer isophotes are much more face-on. Therefore, the kinematic value of the inclination is adopted here.

**NGC 2442.** The peculiar spiral galaxy NGC 2442 is tidally distorted (Pancoast et al. 2010, and references therein).

**NGC 3227.** NGC 3227 is a nearby Seyfert galaxy that is interacting with its gas-poor dwarf elliptical companion NGC 3226. Mundell et al. (1995) discovered a cloud of H I close to, but physically and kinematically distinct from, the galactic disk of NGC 3227. They suggested that this cloud (J1023+1952) might be a dwarf galaxy that is either preexisting and being accreted by NGC 3227, or a newly created tidal dwarf galaxy (Mundell et al. 1995, 2004). However, the oxygen abundance of the cloud (H II regions 24 and 25 from Werk et al. (2011) and of the H II region measured by Lisenfeld et al. (2008)) follows the general trend of the radial abundance distribution in the disk of NGC 3227. The oxygen abundances of the H II region in the cloud estimated in different ways using the emission line measurements by Lisenfeld et al. (2008) are in satisfactory agreement to each other:  $12+\log(\text{O}/\text{H})_{\text{CON}} = 8.40$ ,  $12+\log(\text{O}/\text{H})_{\text{CNS}} = 8.43$  and  $12+\log(\text{O}/\text{H})_P = 8.34$ . H II regions 10 and 12 from Werk et al. (2011) follow also the general trend of the radial abundance distribution in the disk of NGC 3227 although those H II regions may be associated with NGC 3226.

**NGC 3239.** The irregular galaxy NGC 3239 is a candidate for a merging system (Krienke & Hodge 1990). The oxygen abundances determined in four H II regions from SDSS spectra as well as the global abundance determined using the integrated spectra from Moustakas & Kennicutt (2006a) are  $12+\log(\text{O}/\text{H}) \sim 8.0 \div 8.1$ , i.e., those abundances correspond to the transition zone between the upper and lower branches of the  $\text{O}/\text{H} - R_{23}$  diagram. Therefore, the  $(\text{O}/\text{H})_P$  abundances we derived from measurements by Werk et al. (2011) are not reliable and were not used.



**NGC 3310.** NGC 3310 is believed to be an advanced merger and its unusual outer structure is probably the result of a recent merger with a smaller galaxy (Conselice et al. 2000; Knapen & James 2009). Spectroscopic observations of six H II regions in NGC 3310 were presented by Pastoriza et al. (1993). The auroral line [O III] $\lambda$ 4363 is detected in four H II regions. The  $T_e$ -based abundances in those H II regions are in the range from  $12+\log(\text{O}/\text{H}) = 8.13$  to  $8.25$ . However, the coordinates of the H II regions are not published, which prevents us from using those H II regions in radial gradient determinations.

**NGC 3359.** The NGC 3359 is a giant, very strongly barred spiral galaxy. Martin & Roy (1995) estimated the radial gradient using the [O III]/H $\beta$  and [N II]/[O III] indicators (one-dimensional calibrations). They found the radial abundance gradient break near the corotation radius. Zahid & Bresolin (2011) carried out new measurements and determined abundances through the  $N2$  and  $O3N2$  calibrations following Pettini & Pagel (2004). They concluded that, with a high degree of confidence, a model with a break fits the data significantly better than one without a break. The  $C$ -based abundances show no gradient across the entire galaxy. The  $T_e$ -based abundances in three H II regions in NGC 3359 are in agreement with no gradient.

**NGC 3718.** This galaxy is so peculiar that it is difficult to categorize it morphologically (Tully et al. 1996).

**NGC 4559.** The H II regions in NGC 4559 with galactocentric radii larger than  $0.4R_{25}$  measured by Zaritsky et al. (1994) were excluded since they are in the transition zone.

**NGC 4625.** This is a Magellanic spiral with  $R_{25} \sim 3$  kpc and an extended faint disk reaching four times the optical  $R_{25}$  radius of the galaxy in the ultraviolet.

**NGC 5668.** Marino et al. (2012) have found that within  $\sim 36''$  of the nucleus the oxygen abundance O/H follows an exponential profile while the outer abundance trend

flattens out to an approximately constant value and could even reverse.

**NGC 7518.** This is a hydrogen-deficient galaxy in the Pegasus cluster. Following Robertson et al. (2012), oxygen lines from “blue” spectra (360 nm – 560 nm) have been used in the abundance determinations.

**NGC 7529.** This galaxy of the Pegasus cluster has a normal H I content. There is no determination of the position angle, but the inclination is small. Again following Robertson et al. (2012), oxygen lines from “blue” spectra have been used in the abundance determinations.

**NGC 7591.** This galaxy of the Pegasus cluster has a normal H I content. As before, following Robertson et al. (2012), oxygen lines from “blue” spectra have been used in the abundance determinations.

**IC 10.** Due to uncertainties in the position angle and in the inclination of IC 10, the galactocentric distances of H II regions have been computed without any de-projection (following Magrini & Gonçalves 2009).

**IC 5309.** A hydrogen-deficient galaxy of the Pegasus cluster. Following Robertson et al. (2012), oxygen lines from “blue” spectra have been used in the abundance determinations.

**UGC 9562 = II Zw 71.** The blue compact dwarf galaxy UGC 9562 is a probable polar-ring galaxy, and there are a several luminous H II regions along its major axis. The oxygen abundances in four H II regions are around  $12+\log(\text{O}/\text{H}) \sim 8.2$ , i.e., those abundances correspond to the transition zone between the upper and lower branches of the  $\text{O}/\text{H} - R_{23}$  diagram. Therefore, the  $(\text{O}/\text{H})_P$  abundances obtained with measurements from Werk et al. (2011) were not used. The global oxygen abundances determined from the integrated spectra from Kong et al. (2002) are  $12+\log(\text{O}/\text{H}) \sim 8.3$ .

**PGC 029167.** The dwarf galaxy “Garland” or PGC 029167 (a tidal dwarf candidate; Makarova et al. 2002) lies within the tidal bridges of neutral hydrogen connecting M 81, M 82 and NGC 3077. This alignment has led to the suggestion that this dwarf formed recently, as a result of tidal interactions within the group. H II regions in and near Garland exhibit enhanced metallicities compared to other galaxies at similar luminosities. Notably, the oxygen abundances are similar to abundances measured in M 81 and NGC 3077 (Croxall et al. 2009, and references therein).

### 4.3. Properties of abundances in the disks of nearby galaxies

#### 4.3.1. $N/H$ vs. $O/H$

Figure 2 shows the nitrogen abundance as a function of oxygen abundance in our sample of galaxies. The plus signs are the nitrogen  $(N/H)_{R_0}$  and oxygen abundances  $(O/H)_{R_0}$  at  $R_0 = 0$ , i.e., the central nitrogen and oxygen abundances. The points show the nitrogen  $(N/H)_{R_{25}}$  and oxygen  $(O/H)_{R_{25}}$  abundances at the  $R_{25}$  radius of the galaxies. Our data show a well-defined sequence in the  $O/H - N/H$  plot. This sequence exhibits the well-known turnover in the sense that the slope at low metallicity is shallower than that at high metallicity. The commonly accepted explanation of this change of slope is that nitrogen can be interpreted as having both primary and secondary components. Nitrogen production is primary at low metallicity, but for  $12 + \log(O/H) \gtrsim 8.3$ , secondary nitrogen becomes prominent, and nitrogen increases at a faster rate than oxygen (Henry et al. 2000).

Figure 2 shows that at high metallicity,  $12 + \log(O/H) \gtrsim 8.2$ , the relation between the logarithms of nitrogen and oxygen abundances can be approximated by a linear expression. For  $(N/H)_{R_0}$  and  $(O/H)_{R_0}$  abundances, we found the following relation through the least

squares method:

$$\begin{aligned} 12 + \log(\text{N}/\text{H})_{R_0} &= 2.47 (\pm 0.06) \times (12 + \log(\text{O}/\text{H})_{R_0}) \\ &- 13.43 (\pm 0.50). \end{aligned} \quad (7)$$

A similar relation

$$\begin{aligned} 12 + \log(\text{N}/\text{H})_{R_{25}} &= 2.50 (\pm 0.10) \times (12 + \log(\text{O}/\text{H})_{R_{25}}) \\ &- 13.66 (\pm 0.86) \end{aligned} \quad (8)$$

was obtained for the  $(\text{N}/\text{H})_{R_{25}}$  and  $(\text{O}/\text{H})_{R_{25}}$  abundances. A comparison between Eq. (7) and Eq. (8) shows that the relations  $\text{N}/\text{H} = f(\text{O}/\text{H})$  for the  $(\text{N}/\text{H})_{R_0}$  and  $(\text{O}/\text{H})_{R_0}$  abundances and for the  $(\text{N}/\text{H})_{R_{25}}$  and  $(\text{O}/\text{H})_{R_{25}}$  abundances agree with each other within the errors. The  $\text{N}/\text{H} = f(\text{O}/\text{H})$  relation given by Eq. (7) is presented in Figure 2 by the solid line. The dashed lines indicate shifts along the Y-axis by  $\pm 0.15$  dex. At low metallicity,  $12 + \log(\text{O}/\text{H}) \lesssim 8.0$ , the single relation

$$12 + \log(\text{N}/\text{H}) = 0.96 (\pm 0.08) \times (12 + \log(\text{O}/\text{H})) - 1.20 (\pm 0.65) \quad (9)$$

was found using both central abundances and abundances at the  $R_{25}$  radii of the galaxies. This relation is presented in Figure 2 by the dotted line.

Figure 2 shows that there is an appreciable spread in  $\text{N}/\text{H}$  at a given  $\text{O}/\text{H}$ . The variation in  $\text{N}/\text{H}$  is around a factor of 2 for a given  $\text{O}/\text{H}$ . The scatter can be partially attributed to the errors in the abundance determinations but part of it seems to be true abundance scatter. Two major mechanisms have been proposed for generating a spread. One mechanism invokes a time delay between ejections of the freshly manufactured oxygen and nitrogen into the interstellar medium by a given stellar generation. The  $\text{N}/\text{O}$  ratios may be an indicator of the age of a galactic system, indicating the time that has passed since the bulk of star formation activity (Edmunds & Pagel 1978). Thus, the  $\text{N}/\text{O}$  ratio in a galaxy would then depend on its star formation history. The second mechanism for

causing N/H variations at a given O/H is a variation in the efficiency of enriched galactic winds (Pilyugin 1993) or/and in the inflow of gas into the galaxy (Henry et al. 2000). It is believed that galactic winds do not play a significant role in the chemical evolution of large spiral galaxies (Tremonti et al. 2004; Dalcanton 2007). The enhanced N/O ratio in individual H II regions can be caused by the local pollution in nitrogen by Wolf-Rayet stars (López-Sánchez & Esteban 2010, and references therein). Since we consider “average” N and O abundances based on the abundances of different H II regions this origin of the scatter in our diagrams seems to be unlikely.

It has been known for a long time that galaxies of different morphological types have different star formation histories, i.e., spiral galaxies with early morphological types have a larger fraction of old stars (Sandage 1986). One can then expect that N/H at a given O/H may depend on the morphological type of galaxy expressed in terms of  $T$  type (Pilyugin et al. 2003). On the other hand, the star formation history of a galaxy also strongly depends on its mass (or luminosity) as is epitomized in the galaxy downsizing effect, where the star formation activity shifts from high-mass galaxies at early cosmic times to lower-mass galaxies at later epochs (Cowie et al. 1996). Again, one can expect then that the N/H ratio at a given O/H will depend on the galaxy mass (Pilyugin & Thuan 2011).

There is a relatively tight linear correlation between the absolute magnitudes and the logarithms of the linear diameters of nearby galaxies (van den Bergh 2008). Therefore, the linear diameter of a galaxy can be used as indicator of its luminosity (and mass). Thus, if the spread in N/H at a given O/H is caused by the time delay between nitrogen and oxygen enrichment and the different star formation histories in different galaxies then the N/H at a given O/H should correlate with morphological  $T$  type or/and with linear radius of the galaxy.

Figure 3 shows the residual of Eqs. (7),(8) as a function of the morphological  $T$  type

and linear radius of the galaxy  $R_{25}$ . Figure 3 indicates that there may exist some correlation between the N/H at a given O/H and morphological type or/and linear radius of the galaxy. To verify this, we found a relation between N/H and O/H for spiral galaxies (with  $T < 7.5$ ) where  $T$  and  $\log R_{25}$  are “secondary parameters”,  $N/H = f(O/H, T, \log R_{25})$ . It should be noted that  $T$  and  $\log R_{25}$  are not a perfectly independent parameters since there is some correlation between them. The relation obtained for central abundances is

$$\begin{aligned} 12 + \log(N/H)_{R_0} = & -12.67 + 2.39 (12 + \log(O/H)_{R_0}) \\ & - 0.022 T + 0.023 \log(R_{25}). \end{aligned} \quad (10)$$

The values of the coefficients in the terms containing  $T$  and  $\log R_{25}$  are similar. However, the  $T$  value is a more important second parameter than the  $\log R_{25}$  value since the variation in  $T$  values (from 1 to 7.5) is much larger than the variation of  $\log R_{25}$  values (from  $\sim 0.6$  to  $\sim 1.5$ ). Therefore, the variation in N/H due to variation in the morphological type is larger than that due to variation in the linear radii of galaxies. For example, the Sab galaxies ( $T = 2$ ) have nitrogen abundances larger than on average 0.1 dex (i.e., by around 30%) than Sd ( $T = 7$ ) galaxies with the same oxygen abundances. The relation  $N/H = f(O/H, T, \log R_{25})$  obtained for abundances at the optical  $R_{25}$  radii of the galaxies is

$$\begin{aligned} 12 + \log(N/H)_{R_{25}} = & -14.67 + 2.59 (12 + \log(O/H)_{R_{25}}) \\ & + 0.013 T + 0.178 \log(R_{25}). \end{aligned} \quad (11)$$

In this case the  $\log R_{25}$  value is the more important second parameter than the  $T$  value. Although the morphological type is the more important second parameter in the relation for central abundances while  $\log R_{25}$  is the more important second parameter in the relation for abundances at the optical  $R_{25}$  radii of the galaxies, it is difficult to draw a solid conclusion whether this is physically meaningful since there is a correlation between  $T$  and  $\log R_{25}$ . That the relation between N/H and O/H depends on the additional parameter(s)  $T$  and/or  $\log R_{25}$  suggests that the scatter in N/H at a given O/H can be caused, at least partly, by

the time delay between nitrogen and oxygen enrichment and the different star formation histories in different galaxies.

#### 4.3.2. *Abundances and gradients as a function of morphological type and galaxy radius*

The upper left panel of Figure 4 shows the central oxygen  $(\text{O}/\text{H})_{R_0}$  abundance in a galaxy as a function of its morphological  $T$  type (data from Table 1 and Table 2). The  $(\text{O}/\text{H})_{R_0} - T$  diagram shows that there is a trend in central oxygen abundance with morphological type for galaxies later than Sc ( $T \gtrsim 5$ ) such that the central oxygen abundances are lower in galaxies of later types. This trend disappears for early-type spiral galaxies ( $T \lesssim 5$ ).

The upper right panel of Figure 4 shows the central oxygen abundance in a galaxy as a function of its isophotal radius  $R_{25}$ . Since there is a relatively tight linear correlation between the absolute magnitudes and the logarithms of the linear diameters of nearby galaxies (van den Bergh 2008), this diagram can be considered as some kind of analog of the standard “luminosity – metallicity” diagram. The  $(\text{O}/\text{H})_{R_0} - R_{25}$  diagram shows that there is a weak correlation between the central oxygen abundance and optical radius for small galaxies ( $R_{25} \lesssim 10$  kpc) in the sense that the smaller galaxies have on average lower oxygen abundances. This correlation disappears for large galaxies ( $R_{25} \gtrsim 10$  kpc), i.e., the most oxygen-rich galaxies of different radii have similar central oxygen abundances.

Different versions of the luminosity – metallicity diagram have been constructed in earlier studies.  $B$ -band luminosity – characteristic oxygen abundance diagrams were considered in Zaritsky et al. (1994); Pilyugin et al. (2004); Moustakas et al. (2010), where the characteristic oxygen abundance is defined as the abundance at  $R = 0.4R_{25}$ . Tremonti et al. (2004) have used the global abundances (in the sense that their abundances

do not correspond to the abundances at a fixed galactocentric distance, but instead are some kind of mean abundance for a fraction of a galaxy within the fiber aperture) estimated from SDSS spectra in constructing the luminosity – metallicity diagram. The luminosity – central metallicity diagram was examined in Pilyugin et al. (2007). The flattening of the luminosity – metallicity relation at high luminosities (essentially a plateau) can be seen in all versions of the diagram. Thus the plateau in our  $(\text{O}/\text{H})_{R_0} - R_{25}$  diagram at large radii is consistent with previous results.

It has been advocated that the constant maximum value of the observed central oxygen abundance in the most oxygen-rich galaxies suggests that the observed oxygen abundance in the centers of those galaxies represents the maximum attainable value of the gas-phase oxygen abundance (Pilyugin et al. 2007). The upper-row panels of Figure 4 show that the observed central oxygen abundance in the most oxygen-rich galaxies in our sample is  $12 + \log(\text{O}/\text{H})_{R_0} \sim 8.85$ . The dashed lines in the upper row of panels of Figure 4 show this value of oxygen abundance, which seems to correspond to the maximum attainable value of the gas-phase oxygen abundance in galaxies. The observed central oxygen abundance in the most oxygen-rich galaxies from our sample is a factor  $\sim 2$  higher than the gas-phase oxygen abundance in the solar neighbourhood,  $12 + \log(\text{O}/\text{H}) \sim 8.5$  (e.g., Pilyugin et al. 2006). The maximum attainable value of the oxygen abundance in galaxies obtained here is in agreement with the value from Pilyugin et al. (2007). Because some fraction of the oxygen (about 0.1 dex) is expected to be locked in dust grains (e.g., Esteban et al. 1998), the maximum value of the true (gas + dust) oxygen abundances in H II regions of spiral galaxies is  $12 + \log(\text{O}/\text{H})_{R_0} \sim 8.95$ .

The lower left panel of Figure 4 shows the central nitrogen  $(\text{N}/\text{H})_{R_0}$  abundance in a galaxy disk as a function of its morphological  $T$  type. The comparison of the panels in the left column of Figure 4 shows that the changes in the central oxygen and nitrogen



abundances with morphological type of a galaxy are rather similar. The lower right panel of Figure 4 shows the central nitrogen abundance in a galaxy disk as a function of its optical isophotal radius  $R_{25}$ . Again, the comparison between the right column panels of Figure 4 indicates that the general behaviour of the central nitrogen abundances as a function of optical radius is similar to that for oxygen.

According to the relation between nitrogen and oxygen abundances given in Eq. (7), the value of  $12 + \log(\text{N}/\text{H})_{R_0} \sim 8.42$  corresponds to the maximum attainable value of the gas-phase oxygen abundance in galaxies with  $12 + \log(\text{O}/\text{H})_{R_0} \sim 8.85$ . This value of nitrogen abundance is indicated in the lower row of panels of Figure 4 by the dashed lines. One can see that the value of  $12 + \log(\text{N}/\text{H})_{R_0} \sim 8.42$  can be adopted as the maximum value of the observed central nitrogen abundance in the most nitrogen-rich galaxies at the present-day epoch. However, in contrast to the case of oxygen, it is not necessary that this value corresponds to the the maximum attainable value of the gas-phase oxygen abundance in galaxies because of the time-delay between nitrogen and oxygen enrichment of the interstellar medium.

The panels in the left column of Figure 5 show the oxygen  $(\text{O}/\text{H})_{R_{25}}$  (upper panel) and nitrogen  $(\text{N}/\text{H})_{R_{25}}$  (lower panel) abundances measured at the isophotal radius,  $R_{25}$ , as a function of morphological  $T$  type. A comparison between the panels in the left column of Figure 4 and Figure 5 shows that the changes in the central oxygen (nitrogen) abundances and in the abundances at the optical edge of the disk along the Hubble sequence (or morphological type) are more or less similar (at least qualitatively). However, the oxygen and nitrogen abundances at the  $R_{25}$  radius in four of the late-type galaxies (NGC 4625, IC 10, UGC 223, and PGC 29167) are high and those galaxies show a large deviation from the general trends. NGC 4625 is a Magellanic spiral with  $R_{25} \sim 3$  kpc and a very extended faint disk (see below). The dwarf irregular galaxy IC 10 has a very small optical

radius,  $R_{25} = 0.6$  kpc, and a positive radial abundance gradient. One may suggest though that any radial gradient in such small galaxies is hard to define based on H II regions. It remains a mystery why the oxygen abundance changes by a factor of about two on the scale of 0.6 kpc in this galaxy. IC 10 is one of several dwarf galaxies in which evidence for localized, inhomogeneous enrichment has been found (Kniazev et al. 2005; Koch et al. 2008b,a; Magrini & Gonçalves 2009; López-Sánchez et al. 2011) – perhaps this is a common mode of enrichment in these small objects. In contrast, the irregular galaxy UGC 223 is rather large with  $R_{25} = 9.3$  kpc. The peculiar dwarf galaxy PGC 29167 (or “Garland”) is commonly considered a tidal dwarf galaxy (see comment on this galaxy in Section 4.2).

The panels in the right column of Figure 5 show the oxygen  $(\text{O}/\text{H})_{R_{25}}$  (upper panel) and nitrogen  $(\text{N}/\text{H})_{R_{25}}$  (lower panel) abundances at the optical edge of the disk as defined by the  $R_{25}$  radius as a function of isophotal radius  $R_{25}$ . The positions of the galaxies in the  $(\text{O}/\text{H})_{R_{25}} - R_{25}$  and  $(\text{N}/\text{H})_{R_{25}} - R_{25}$  diagrams do not show any obvious trends. In particular, the  $(\text{O}/\text{H})_{R_{25}}$  and  $(\text{N}/\text{H})_{R_{25}}$  abundances do not show any appreciable correlation with isophotal radius  $R_{25}$ . However, one feature in these diagrams should be noted: the  $(\text{O}/\text{H})_{R_{25}}$  and  $(\text{N}/\text{H})_{R_{25}}$  abundances have a maximum value in galaxies with an isophotal radius  $R_{25} \sim 10$  kpc and decrease when moving from this value both towards smaller or larger optical radii.

Figure 6 shows the radial oxygen and nitrogen abundance gradients in units of  $\text{dex kpc}^{-1}$  as a function of morphological  $T$  type (left panels) and of isophotal radius  $R_{25}$  of a galaxy (right panels). Inspection of the left column panels of Figure 5 shows that the values of the abundance gradients in units of  $\text{dex kpc}^{-1}$  do not correlate with the morphological type of a galaxy. According to Zaritsky et al. (1994), the lack of a correlation between gradients in units of  $\text{dex kpc}^{-1}$  and the macroscopic properties of late-type galaxies may suggest that the relationship between these parameters is more complex than a simple

correlation. Indeed, Vila-Costas & Edmunds (1992) have concluded that a correlation for non-barred galaxies is seen. The panels in the right column of Figure 5 show that shallow gradients can be found both in small and large galaxies while steep gradients are seen only in small galaxies in the sense that the smaller a galaxy the steeper its gradient.

## 5. Summary

We compiled published spectra of H II regions in 130 nearby galaxies. Our list contains 3904 spectra including 162 spectra of H II regions beyond the isophotal radius  $R_{25}$ . The oxygen and nitrogen abundances in H II regions were determined on the metallicity scale defined by H II regions with  $T_e$ -based abundances. The radial gradients of oxygen and nitrogen abundances across the disks of the galaxies were estimated.

At the centers of metal-rich galaxies (i.e.,  $(12 + \log(\text{O}/\text{H})) \gtrsim 8.2$ ), we found the relation between N and O abundances to be  $(\text{N}/\text{H})_{R_0} \propto (\text{O}/\text{H})_{R_0}^{2.5}$ . The  $(\text{N}/\text{H})_{R_{25}} = f(\text{O}/\text{H})_{R_{25}}$  relation between N and O abundances at the  $R_{25}$  isophotal radii of high metallicity galaxies is similar to that for the abundances at their centers. The variation in  $(\text{N}/\text{H})$  at a given  $(\text{O}/\text{H})$  is around 0.3 dex. To test whether the scatter in  $\text{N}/\text{H}$  at a given  $\text{O}/\text{H}$  can be explained by the time delay between nitrogen and oxygen enrichment and the different star formation histories in galaxies of different morphological types and dimensions (masses), we derived a more complex relation between N and O abundances  $(\text{N}/\text{H}) = f((\text{O}/\text{H}), T, R_{25})$ . We found that the morphological type,  $T$ , is a more important “second parameter” in the relation for central abundances, while the  $\log R_{25}$  is a more important second parameter in the relation for abundances at the  $R_{25}$  radii of our galaxies. Since there is a correlation between  $T$  and  $\log R_{25}$  it is as yet unclear whether this difference is meaningful. The fact that the relation between  $\text{N}/\text{H}$  and  $\text{O}/\text{H}$  depends on additional parameter(s), namely  $T$  and/or  $\log R_{25}$  suggests that the scatter in  $\text{N}/\text{H}$  at a given  $\text{O}/\text{H}$  can be caused, at least

partly, by the time delay between nitrogen and oxygen enrichment and the different star formation histories in different galaxies. The best fit to N/H as a function of O/H is close to a linear relation at low metallicity ( $12 + \log(\text{O}/\text{H}) \lesssim 8.0$ ).

The central oxygen abundances  $(\text{O}/\text{H})_{R_0}$  show a trend along the Hubble sequence of galaxies of late morphological types ( $T \gtrsim 5$ ) such that the oxygen abundances are lower in galaxies of later types. This trend disappears for early morphological types. The central oxygen abundance also correlates with optical galaxy radius for small galaxies,  $R_{25} \lesssim 10$  kpc, being lower in galaxies of smaller radii. The trend disappears for galaxies with large radii. The maximum gas-phase oxygen abundance in large ( $10 \text{ kpc} \lesssim R_{25} \lesssim 30 \text{ kpc}$ ) galaxies (or in galaxies of early ( $1 \lesssim T \lesssim 5$ ) morphological types) is constant,  $12 + \log(\text{O}/\text{H}) \sim 8.85$ . This implies that the observed central oxygen abundance of the most oxygen-rich galaxies in our sample is a factor of  $\sim 2$  higher than the gas-phase oxygen abundance in the solar neighbourhood. The central nitrogen abundances  $(\text{N}/\text{H})_{R_0}$  show a similar behaviour. The observed central nitrogen abundance in the most nitrogen-rich galaxies of our sample is  $12 + \log(\text{O}/\text{H}) \sim 8.42$ .

The radial O and N abundance gradients (in units of  $\text{dex kpc}^{-1}$ ) within the optical radius do not show any significant correlation with the morphological type and optical radius. However, the spread in the gradients increases with decreasing galaxy radius in the sense that shallow gradients are seen both in small and large galaxies while steep gradients occur only in a small galaxies. The smaller a galaxy the steeper is the gradient that it may show.

The abundance data set presented in this paper serves as the foundation for other investigations we are carrying out. In a forthcoming paper (Pilyugin et al. 2014), we examine relations between the radial abundance distribution across the disk and the disk surface brightness profiles in the optical  $B$  and infrared  $K$  bands for a sample of nearby

galaxies.

### Acknowledgements

We are grateful to the referee for his or her constructive comments.

L.S.P. and E.K.G. acknowledge support within the framework of Sonderforschungsbereich (SFB 881) on “The Milky Way System” (especially subproject A5), which is funded by the German Research Foundation (DFG). L.S.P. thanks the Astronomisches Rechen-Institut at Heidelberg University where this investigation was carried out for the hospitality. A.Y.K. acknowledges the support from the National Research Foundation (NRF) of South Africa. We thank H.J. Zahid and F. Bresolin for supporting us with some unpublished details of their observations of H II regions in NGC 3359.

The authors acknowledge the work of the SDSS collaboration. Funding for SDSS-III has been provided by the Alfred P. Sloan Foundation, the Participating Institutions, the National Science Foundation, and the U.S. Department of Energy Office of Science. The SDSS-III web site is <http://www.sdss3.org/>. SDSS-III is managed by the Astrophysical Research Consortium for the Participating Institutions of the SDSS-III Collaboration including the University of Arizona, the Brazilian Participation Group, Brookhaven National Laboratory, University of Cambridge, Carnegie Mellon University, University of Florida, the French Participation Group, the German Participation Group, Harvard University, the Instituto de Astrofísica de Canarias, the Michigan State/Notre Dame/JINA Participation Group, Johns Hopkins University, Lawrence Berkeley National Laboratory, Max Planck Institute for Astrophysics, Max Planck Institute for Extraterrestrial Physics, New Mexico State University, New York University, Ohio State University, Pennsylvania

State University, University of Portsmouth, Princeton University, the Spanish Participation Group, University of Tokyo, University of Utah, Vanderbilt University, University of Virginia, University of Washington, and Yale University.

We acknowledge the usage of the HyperLeda database (<http://leda.univ-lyon1.fr>).

## REFERENCES

- Alloin, D., Collin-Souffrin, S., Joly, M., & Vigroux, L. 1979, *A&A*, 78, 200
- Alloin, D., Edmunds, M. G., Lindblad, P. O., & Pagel, B. E. J. 1981, *A&A*, 101, 377
- Amram, P., Le Coarer, E., Marcelin, M., et al. 1992, *A&AS*, 94, 175
- Amram, P., Marcelin, M., Balkowski, C., et al. 1994, *A&AS*, 103, 5
- Ball, R. 1986, *ApJ*, 307, 453
- Barberá, C., Athanassoula, E., & García-Gómez C. 2004, *A&A*, 415, 849
- Barbieri, C. V., Fraternali, F., Oosterloo, T., et al. 2005, *A&A*, 439, 947
- Begum, A., & Chengalur, J. N. 2003, *A&A*, 409, 879
- Berg, D. A., Skillman, E. D., Marble, A. R., et al. 2012, *ApJ*, 754, 98
- Bibby, J. L., & Crowther, P. A. 2010, *MNRAS*, 405, 2737
- Blair, W. P., Kirshner, R. P., & Chevalier, R. A. 1982, *ApJ*, 254, 50
- Blais-Ouellette, S., Amram, P., Carignan, C., & Swaters, R. 2004, *A&A*, 420, 147
- Bono, G., Caputo, F., Marconi, M., & Musella, I. 2010, *ApJ*, 715, 277
- Boomsma, R., Oosterloo, T. A., Fraternali, F., van der Hulst, J. M., & Sancisi, R. 2008, *A&A*, 490, 555
- Bresolin, F. 2007, *ApJ*, 656, 186
- Bresolin, F., & Kennicutt, R. C., 2002, *ApJ*, 572, 838
- Bresolin, F., Kennicutt, R. C., & Garnett, D. R., 1999, *ApJ*, 510, 104

- Bresolin, F., Garnett, D. R., & Kennicutt, R. C. 2004, *ApJ*, 615, 228
- Bresolin, F., Schaerer, D., González Delgado, R. M., & Stasińska, G. 2005, *A&A*, 441, 981
- Bresolin, F., Gieren, W., Kudritzki, R.-P., et al. 2009a, *ApJ*, 700, 309
- Bresolin, F., Ryan-Weber, E., Kennicutt, R. C., & Goddard, Q. 2009b, *ApJ*, 695, 580
- Bresolin, F., Stasińska, G., Vílchez, J. M., Simon, J. D., & Rosolowsky, E. 2010, *MNRAS*, 404, 1679
- Bresolin, F., Kennicutt, R. C., & Ryan-Weber, E., 2012, *ApJ*, 750, 122
- Bush, S. J., & Wilcots, E. M. 2004, *AJ*, 128, 2789
- Carignan, C. 1985, *ApJS*, 58, 107
- Conselice, C., Gallagher, J. S., Calzetti, D., Homeier, N., & Kinney A. 2000, *AJ*, 119, 79
- Cowie, L. L., Songaila, A., Hu, E. M., & Cohen, J. G. 1996, *AJ*, 112, 839
- Crosthwaite, L. P., Turner, J. L., & Ho, P. T. P. 2000, *AJ*, 119, 1720
- Croxall, K. V., van Zee, L., Lee, H., et al. 2009, *ApJ*, 705, 723
- Dalcanton, J. J. 2007, *ApJ*, 658, 941
- Dalcanton, J. J., Williams, B. F., Seth, A. C., et al. 2009, *ApJS*, 183, 67
- de Blok, W. J. G., & Bosma, A. 2002, *A&A*, 385, 816
- de Blok, W. J. G., Walter, F., Brinks, E., et al. 2008, *AJ*, 136, 2648
- Dennefeld, M., & Kunth, D. 1981, *AJ*, 86, 989
- Dessart, L., Blondin, S., Brown, P. J., et al. 2008, *ApJ*, 675, 644



- de Vaucouleurs, G., de Vaucouleurs, A., Corvin, H. G., et al. 1991, Third Reference Catalog of Bright Galaxies, New York: Springer Verlag (RC3)
- Díaz, A. I., Terlevich, E., Pagel, B. E. J., Vilchez, J. M., & Edmunds, M. G. 1987, MNRAS, 226, 19
- Díaz, A. I., Terlevich, E., Vilchez, J. M., Pagel, B. E. J., & Edmunds, M. G. 1991, MNRAS, 253, 245
- Díaz, A. I., Castellanos, M., Terlevich, E., & García-Vargas, M. L. 2000, MNRAS, 318, 462
- Díaz, Á. I., Terlevich, E., Castellanos, M., & Hägele, G. F. 2007, MNRAS, 382, 251
- Dicaire, I., Carignan, C., Amram, P., et al. 2008, MNRAS, 385, 553
- Dinerstein, H. L., & Shields, G. A., 1986, ApJ, 311, 45
- Dopita, M. A., & Evans, I. N. 1986, ApJ, 307, 431
- Drozdovsky, I. O., & Karachentsev, I. D. 2000, A&AS, 142, 425
- Dufour, R. J., Talbot, R. J., Jensen, E. B., & Shields, G. A. 1980, ApJ, 236, 119
- Edmunds, M. G., & Pagel, B. E. J. 1978, MNRAS, 185, 77
- Edmunds, M. G., & Pagel, B. E. J. 1984, MNRAS, 211, 507
- Epinat, B., Amram, P., & Marcelin, M. 2008, MNRAS, 390, 466
- Esteban, C., Peimbert, M., Torres-Peimbert, S., & Escalante, V. 1998, MNRAS, 295, 401
- Esteban, C., Bresolin, F., Peimbert, M., et al. 2009, ApJ, 700, 654
- Evans, I. N., & Dopita, M. A. 1987, ApJ, 319, 662
- Ferguson, A. M. N., Gallagher, J. S., & Wyse, R. F. G. 1998, AJ, 116, 673

- Fernandes, I. F., de Carvalho, R., Contini, T., & Gal, R. R. 2004, MNRAS, 355, 728
- Fierro, J., Torres-Peimbert, S., & Peimbert, M. 1986, PASP, 98, 1032
- Firpo, V., Bosch, G., & Morrell, N. 2005, MNRAS, 356, 1357
- Galarza, V. C., Walterbos, R. A. M., & Braun, R. 1999, AJ, 118, 2775
- García-Benito, R., Díaz, A. I., Hägele, G. E., et al. 2010, MNRAS, 408, 2234
- García-Gómez, C., Barberá, C., Athanassoula, E., Bosma, A., & Whyte, L. 2004, A&A, 421, 595
- Garnett, D. R., & Kennicutt, R. C. 1994, ApJ, 426, 123
- Garnett, D. R., Kennicutt, R. C., & Bresolin, F. 2004, ApJ, 607, L21
- Garnett, D. R., & Shields, G. A. 1987, ApJ, 317, 82
- Garnett, D. R., Shields, G. A., Peimbert, M., et al. 1999, ApJ, 513, 168
- Garnett, D. R., Shields, G. A., Skillman, E. D., Sagan, S. P., & Dufour, R. J. 1997, ApJ, 489, 63
- Gil de Paz, A., Boissier, S., Madore, B. F., et al. 2007, ApJS, 173, 185
- Goddard, Q., Bresolin, F., Kennicutt, R. C., Ryan-Weber, E. V., & Rosales-Ortega, F. F. 2011, MNRAS, 412, 1246
- González Delgado, R. M., & Pérez, E. 1997, MNRAS, 284, 931
- Grosbøl, P. J. 1985, A&AS, 60, 261
- Gusev, A. S., Pilyugin, L. S., Sakhibov, F., et al. 2012, MNRAS, 424, 1930
- Hadfield, L. J., & Crowther, P. A. 2007, MNRAS, 381, 418

- Hawley, S. A. 1978, *ApJ*, 224, 417
- Henry, R. B. C., Pagel, B. E. J., & Chincarini, G. L. 1994, *MNRAS*, 266, 421
- Henry, R. B. C., Balkowski, C., Cayatte, V., Edmunds, M. G., & Pagel, B. E. J. 1996, *MNRAS*, 283, 635
- Henry, R. B. C., Edmunds, M. G., & Kóppen, J. 2000, *ApJ*, 541, 660
- Herrmann, K. A., & Ciardullo, R. 2009, *ApJ*, 705, 1686
- Herrmann, K. A., Ciardullo, R., Feldmeier, J. J., & Vinciguerra, M. 2008, *ApJ*, 683, 630
- Hess, K. M., Pisano, D. J., Wilcots, E. M., & Chengalur, J. N. 2009, *ApJ*, 699, 76
- Hlavacek-Larrondo, J., Carignan, C., Daigle, O., et al. 2011, *MNRAS*, 411, 71
- Humphreys, E. M. L., Reid, M. J., Greenhill, L. J., Moran, J. M., & Argon, A. L. 2008, *ApJ*, 672, 800
- Izotov, Y. I., Thuan, T. X., & Lipovetsky, V. A. 1994, *ApJ*, 435, 647
- Izotov, Y. I., Thuan, T. X., & Lipovetsky, V. A. 1997, *ApJS*, 108, 1
- Izotov, Y. I., Thuan, T. X., & Stasińska, G. 2007, *ApJ*, 662, 15
- Jacobs, B. A., Rizzi, L., Tully, R. B., et al. 2009, *AJ*, 138, 332
- Jamet, L., Stasińska, G., Pérez, E., González Delgado, R. M., & Vílchez, J. M. 2005, *A&A*, 444, 723
- Kamphuis, J. J. 1993, PhD Thesis, Univ. Groningen
- Kamphuis, J., & Briggs, F. 1992, *A&A*, 253, 335
- Karachentsev, I. D., Dolphin, A. E., Geisler, D., et al. 2002, *A&A*, 383, 125

- Kehrig, C., Ory, M. S., Crowther, P.A., et al. 2011, *A&A*, 526, A128
- Kennicutt, R. C., Bresolin, F., & Garnett, D. R. 2003, *ApJ*, 591, 801
- Kennicutt, R. C., & Garnett, D. R. 1996, *ApJ*, 456, 504
- Kewley, L. J., & Dopita, M. A. 2002, *ApJS*, 142, 35
- Kewley, L. J., & Ellison, S. L. 2008, *ApJ*, 681, 1183
- Kinkel, U., & Rosa, M. R. 1994, *A&A*, 282, L37
- Kirby, E. M., Jerjen, H., Ryder, S. D., & Driver, S. P. 2008, *AJ*, 136, 1866
- Knapen, J. H., & James, P. A. 2009, *ApJ*, 698, 1437
- Kniazev, A. Y., Pustilnik, S. A., Grebel, E. K., Lee, H., & Pramskij, A. G. 2004, *ApJS*, 153, 429
- Kniazev, A. Y., Grebel, E. K., Pustilnik, S. A., Pramskij, A. G., & Zucker, D. B. 2005, *AJ*, 130, 1558
- Kobulnicky, H. A., & Skillman, E. D. 1998, *ApJ*, 497, 601
- Koch, A., Grebel, E. K., Gilmore, G. F., et al. 2008a, *AJ*, 135, 1580
- Koch, A., McWilliam, A., Grebel, E. K., Zucker, D. B., & Belokurov, V. 2008b, *ApJ*, 688, L13
- Kong, X., Cheng, F. Z., Weiss, A., & Charlot, S. 2002, *A&A*, 396, 503
- Kopparapu, R. K., Hanna, C., Kalogera, V., et al. 2008, *ApJ*, 675, 1459
- Krienke, K., & Hodge, P. 1990, *PASP*, 102, 41
- Kwitter, K. B., & Aller, L. H. 1981, *MNRAS*, 195, 939

- Lee, J. C., Gil de Paz, A., Kennicutt, R. C., et al. 2011, *ApJS*, 192, 6
- Lequeux, J., Peimbert, M., Rayo, J. F., Serrano, A., & Torres-Peimbert, S. 1979, *A&A*, 80, 155
- Liang, Y. C., Yin, S. Y., Hammer, F., et al. 2006, *ApJ*, 652, 257
- Lisenfeld, U., Mundell, C. G., Schinnerer, E., Appleton, P. N., & Allsopp, J. 2008, *ApJ*, 685, 181
- López-Sánchez, Á. R., & Esteban, C. 2010, *A&A*, 517, A85
- López-Sánchez, Á. R., Mesa-Delgado, A., López-Martín, L., & Esteban, C. 2011, *MNRAS*, 411, 2076
- López-Sánchez, Á. R., Dopita, M. A., Kewley, L. J., et al. 2012, *MNRAS*, 426, 2630
- Luridiana, V., Esteban, C., Peimbert, M., & Peimbert, A. 2002, *Rev. Mex. A. A.*, 38, 97
- Maeder, A. 1992, *A&A*, 264, 105
- Magrini, L., & Gonçalves, D. R. 2009, *MNRAS*, 398, 280
- Magrini, L., Stanghellini, L., Corbelli, E., Galli, D., & Villaver, E. 2010, *A&A*, 512, A63
- Makarova, L. N., Grebel, E. K., Karachentsev, I. D., et al. 2002, *A&A*, 396, 473
- Marcelin, M., & Athanassoula, E. 1982, *A&A*, 105, 76
- Marcelin, M., Boulesteix, J., & Georgelin, Y. 1983, *A&A*, 128, 140
- Marino, R. A., Gil de Paz, A., Castillo-Morales, A., et al. 2012, *ApJ*, 754, 61
- Martin, P., & Roy, J.-R. 1995, *ApJ*, 445, 161
- McCall, M. L., Rybski, P. M., & Shields, G. A. 1985, *ApJS*, 57, 1

- McGaugh, S. S. 1991, *ApJ*, 380, 140
- Miller, B. W., & Hodge, P. 1996, *ApJ*, 458, 467
- Moles, M., Aparicio, A., & Masegosa, J. 1990, *A&A*, 228, 310
- Moustakas, J., & Kennicutt, R. C. 2006a, *ApJS*, 164, 81
- Moustakas, J., & Kennicutt, R. C. 2006b, *ApJ*, 651, 155
- Moustakas, J., Kennicutt, R. C., Tremonti, C. A., et al. 2010, *ApJS*, 190, 233
- Müller, E., & Höflich, P. 1994, *A&A*, 281, 51
- Mundell, C. G., James, P. A., Loiseau, N., Schinnerer, E., & Forbes, D. A. 2004, *ApJ*, 614, 648
- Mundell, C. G., Pedlar, A., Axon, D. J., Meaburn, J., & Unger, S. W. 1995, *MNRAS*, 277, 641
- Noeske, K. G., Guseva, N. G., Fricke, K. J., et al. 2000, *A&A*, 361, 33
- Oey, M. S., & Kennicutt, R. C. 1993, *ApJ*, 411, 137
- Olivares, E., Hamuy, M., Pignata, G., et al. 2010, *ApJ*, 715, 833
- Ondrechen, M. P., & van der Hulst, J. M. 1989, *ApJ*, 342, 29
- Ondrechen, M. P., van der Hulst, J. M., & Hummel, E. 1989, *ApJ*, 342, 39
- Pagel, B. E. J. 1997, *Nucleosynthesis and Chemical Evolution of Galaxies* (Cambridge: Cambridge Univ. Press)
- Pagel, B. E. J., Edmunds, M. G., Blackwell, D. E., Chun, M. S., & Smith, G. 1979, *MNRAS*, 189, 95

- Pagel, B. E. J., Edmunds, M. G., & Smith, G. 1980, MNRAS, 193, 219
- Pancoast, A., Sajina, A., Lacy, M., Noriega-Crespo, A., & Rho, J. 2010, ApJ, 723, 530
- Pastoriza, M. G., Dottori, H. A., Terlevich, E., Terlevich, R., & Díaz, A. I. 1993, MNRAS, 260, 177
- Patterson, M. T., Walterbos, R. A. M., Kennicutt, R. C., Chiappini, C., & Thilker, D. A. 2012, MNRAS, 422, 401
- Paturel, G., Petit, C., Prugniel, P., et al. 2003, A&A, 412, 45
- Peletier, R. F., Knapen, J. H., Shlosman, I., et al. 1999, ApJS, 125, 363
- Pérez-Montero, E., García-Benito, R., Díaz, A. I., Pérez, E., & Kehrig, C. 2009, A&A, 497, 53
- Petrosian, A., McLean, B., Allen, R. J., & MacKenty, J. W. 2007, ApJS, 170, 33
- Pettini, M., & Pagel, B. E. J. 2004, MNRAS, 348, L59
- Phillips, M. M., Pagel, B. E. J., Edmunds, M. G., & Díaz, A. 1984, MNRAS, 210, 701
- Pietrzyński, G., Gieren, W., Hamuy, M., et al. 2010, AJ, 140, 1475
- Pilyugin, L. S. 1993, A&A, 277, 42
- Pilyugin, L. S. 2000, A&A, 362, 325
- Pilyugin, L. S. 2001, A&A, 369, 594
- Pilyugin, L. S. 2003, A&A, 397, 109
- Pilyugin, L. S., Grebel, E. K., & Mattsson, L. 2012, MNRAS, 424, 2316
- Pilyugin, L. S., Grebel, E. K., Zinchenko, A. I., & Kniazev, A. Y. 2014, AJ, submitted

- Pilyugin, L. S., Lara-López, M.A., Grebel, E. K., et al., 2013, MNRAS, 432, 1217
- Pilyugin, L. S., & Mattsson, L. 2011, MNRAS, 412, 1145
- Pilyugin, L. S., & Thuan, T. X. 2005, ApJ, 631, 231
- Pilyugin, L. S., & Thuan, T. X. 2011, ApJ, 726, L23
- Pilyugin, L. S., Thuan, T. X., & Vílchez, J. M. 2003, A&A, 397, 487
- Pilyugin, L. S., Thuan, T. X., & Vílchez, J. M. 2006, MNRAS, 367, 1139
- Pilyugin, L. S., Thuan, T. X., & Vílchez, J. M. 2007, MNRAS, 376, 353
- Pilyugin, L. S., Vílchez, J. M., & Contini, T. 2004, A&A, 425, 849
- Pilyugin, L. S., Vílchez, J. M., & Thuan, T. X. 2010, ApJ, 720, 1738
- Pisano, D. J., Wilcots, E. M., & Elmegreen, B. G. 1998, AJ, 115, 975
- Pohlen, M., & Trujillo, I. 2006, A&A, 454, 759
- Poznanski, D., Butler, N., Filippenko, A. V., et al. 2009, ApJ, 694, 1067
- Puche, D., Carignan, C., & Wainscoat, R. J. 1991, AJ, 101, 447
- Puche, D., Westpfahl, D., & Brinks, E. 1992, AJ, 103, 1841
- Rayo, J.F., Peimbert, M., & Torres-Peimbert, S. 1982, ApJ, 255, 1
- Relaño, M., Monreal-Ibero, A., Vílchez, J. M., & Kennicutt, R. C. 2010, MNRAS, 402, 1635
- Riad, I. F., Kraan-Kortweg, R. C., & Woudt, P. A. 2010, MNRAS, 401, 924
- Richer, M. G., Bullesos, A., Borissova, J., et al. 2001, A&A, 370, 34
- Robertson, P., Shields, G. A., & Blanc, G. A. 2012, ApJ, 748, 48



- Rodrigues, I., Dottori, H., Cepa, J., & Vilchez, J. M. 1998, A&AS, 128, 545
- Rosales-Ortega, F. F., Kennicutt, R. C., Sánchez, S. F., et al. 2010, MNRAS, 405, 735
- Rosales-Ortega, F. F., Díaz, A. I., Kennicutt, R. C., & Sánchez, S. F. 2011, MNRAS, 415, 2439
- Rownd, B. K., Dickey, J. M., & Helou, G. 1994, AJ, 108, 1638
- Roy, J.-R., & Walsh, J. R. 1997, MNRAS, 288, 715
- Roy, J.-R., Wang, J., & Arsenault, R. 1991, AJ, 101, 825
- Rubin, V. C., Whitmore, B. C., & Ford, W. K. 1988, ApJ, 333, 522
- Ryder, S. D. 1995, ApJ, 444, 610
- Saha, A., Claver, J., & Hoessel, J. G. 2002, AJ, 124, 839
- Saha, A., Thim, F., Tamman, G. A., Reindl, B., & Sandage, A. 2006, ApJS, 165, 108
- Sakai, S., Madore, B. F., & Freedman, W. L. 1999, ApJ, 511, 671
- Sánchez, S.F., Rosales-Ortega, F. F., Marino, R.A., et al. 2012, A&A, 546, A2
- Sandage, A. 1986, A&A, 161, 89
- Sanders, N. E., Caldwell, N., McDowell, J., & Harding, P. 2012, ApJ, 758, 133
- Schmidt, B. P., Kirshner, R. P., Eastman, R. G., et al. 1994, ApJ, 432, 42
- Searle, L. 1971, ApJ, 168, 327
- Sedwick, K. E., & Aller, L. H. 1981, Proc. Nat. Acad. Sci. USA., 78, 1994
- Send, U. 1982, A&A, 112, 235

- Seth, A. C., Dalcanton, J. J., & de Jong, R. S. 2005, *AJ*, 129, 1331
- Sharina, M. E., Karachentsev, I. D., & Tikhonov, N. A. 1997, *Astron. Lett.*, 23, 373
- Shields, G. A., Skillman, E. D., & Kennicutt, R. C. 1991, *ApJ*, 371, 82
- Skillman, E. D. 1985, *ApJ*, 290, 449
- Skillman, E. D., Kennicutt, R. C., Shields, G. A., & Zaritsky, D. 1996, *ApJ*, 462, 147
- Skillman E. D., Salzer, J. J., Berg, D. A., et al. 2013, *AJ*, 146, 3
- Smith, H. E. 1975, *ApJ*, 199, 591
- Stanghellini, L., Magrini, L., Villaver, E., & Galli, D. 2010, *A&A*, 521, A3
- Stasińska, G. 2006, *ApJ*, 454, L127
- Stasińska, G., Comte, G., & Vigroux, L. 1986, *A&A*, 154, 352
- Storchi-Bergmann, T., Rodríguez-Ardila, A., Schmidt, H. R., Wilson, A. S., & Baldwin, J. A. 1996a, *ApJ*, 472, 83
- Storchi-Bergmann, T., Wilson, A. S., & Baldwin, J. A. 1996b, *ApJ*, 460, 252
- Storey, P. J., & Zeippen, C. J. 2000, *MNRAS*, 312, 813
- Springob, C. M., Masters, K. L., Haynes, M. P., Giovanelli, R., & Marinoni, C. 2009, *ApJS*, 182, 474
- Stauffer, J. R., & Bothun, G. D. 1984, *AJ*, 89, 1702
- Swaters, R. A., & Balcells, M. 2002, *A&A*, 390, 863
- Terry, J. N., Paturel, G., & Ekholm, T. 2002, *A&A*, 393, 57

- Thim, F., Hoessel, J. G., Saha, A., et al. 2004, *AJ*, 127, 2322
- Thuan, T. X., Pilyugin, L. S., & Zinchenko, I. A. 2010, *ApJ*, 712, 1029
- Tikhonov, N. A., & Galazoutdinova, O. A. 2002, *Afz*, 45, 253
- Torres-Peimbert, S., Peimbert, M., & Fierro, J. 1989, *ApJ*, 345, 186
- Tremonti, C. A., Heckman, T.M., Kauffmann, G., et al., 2004, *ApJ*, 613, 898
- Tüllmann, R., Rosa, M. R., Elwert, T., et al. 2003, *A&A*, 412, 69
- Tully, R. B. 1988, *Nearby Galaxy Catalogue* (Cambridge Univ. Press, Cambridge)
- Tully, R. B., Verheijen, M. A. W., Pierce, M. J., Huang, J.-S., & Wainscoat, R. J. 1996, *AJ*, 112, 2471
- Tully, R. B., Rizzi, L., Shaya, E. J., et al. 2009, *AJ*, 138, 323
- van Albada, G. D. 1980, *A&A*, 90, 123
- van den Bergh, S. 2008, *A&A*, 490, 97
- van den Hoek, L. B., & Groenewegen, M. A. T. 1997, *A&AS*, 123, 305
- van Zee, L. 2000, *AJ*, 119, 2757
- van Zee, L., & Bryant, J. 1999, *AJ*, 118, 2172
- van Zee, L., & Haynes, M. P. 2006, *ApJ*, 636, 214
- van Zee, L., Salzer, J. J., Haynes, M. P., O’Donoghue, A. A., & Balonek, T. J. 1998, *AJ*, 116, 2805
- van Zee, L., Skillman, E. D., & Haynes, M. P. 2006, *ApJ*, 637, 269

- Verdes-Montenegro, L., Bosma, A., & Athanassoula, E. 2000, *A&A*, 356, 827
- Vila-Costas, M. B., & Edmunds, M. G. 1992, *MNRAS*, 259, 121
- Vilardell, F., Ribas, I., Jordi, C., Fitzpatrick, E. L., & Guinan, E. F. 2010, *A&A*, 509, A70
- Vílchez, J. M., Edmunds, M. G., & Pagel, B. E. J. 1988b, *PASP*, 100, 1428
- Vílchez, J. M., Pagel, B. E. J., Díaz, A. I., Terlevich, E., & Edmunds, M. G. 1988a, *MNRAS*, 235, 633
- Walsh, J. R., & Roy, J.-R. 1997, *MNRAS*, 288, 726
- Walter, F., Brinks, E., de Blok, W. J. G., et al. 2008, *AJ*, 136, 2563
- Walterbos, R. A. M., & Kennicutt, R. C. 1987, *A&AS*, 69, 311
- Webster, B. L., & Smith, M. G. 1983, *MNRAS*, 204, 743
- Werk, J. K., Putman, M. E., Meurer, G. R., & Santiago-Figueroa, N. 2011, *ApJ*, 735, 71
- Whiteoak, J. B., & Gardner, F. F. 1977, *Aust. J. Phys.*, 30, 187
- Wood-Vasey, W. M., Friedman, A. S., Bloom, J. S., et al. 2008, *ApJ*, 689, 377
- York, D. G., Adelman, J., Anderson, J. E., et al. 2000, *AJ*, 120, 1579
- Zahid, H. J., & Bresolin, F. 2011, *AJ*, 141, 192
- Zaritsky, D., Elston, R., & Hill, J. M. 1989, *AJ*, 97, 97
- Zaritsky, D., Elston, R., & Hill, J. M. 1990, *AJ*, 99, 1108
- Zaritsky, D., Kennicutt, R. C., & Huchra, J. P. 1994, *ApJ*, 420, 87
- Zurita, A., & Bresolin, F. 2012, *MNRAS*, 427, 1463



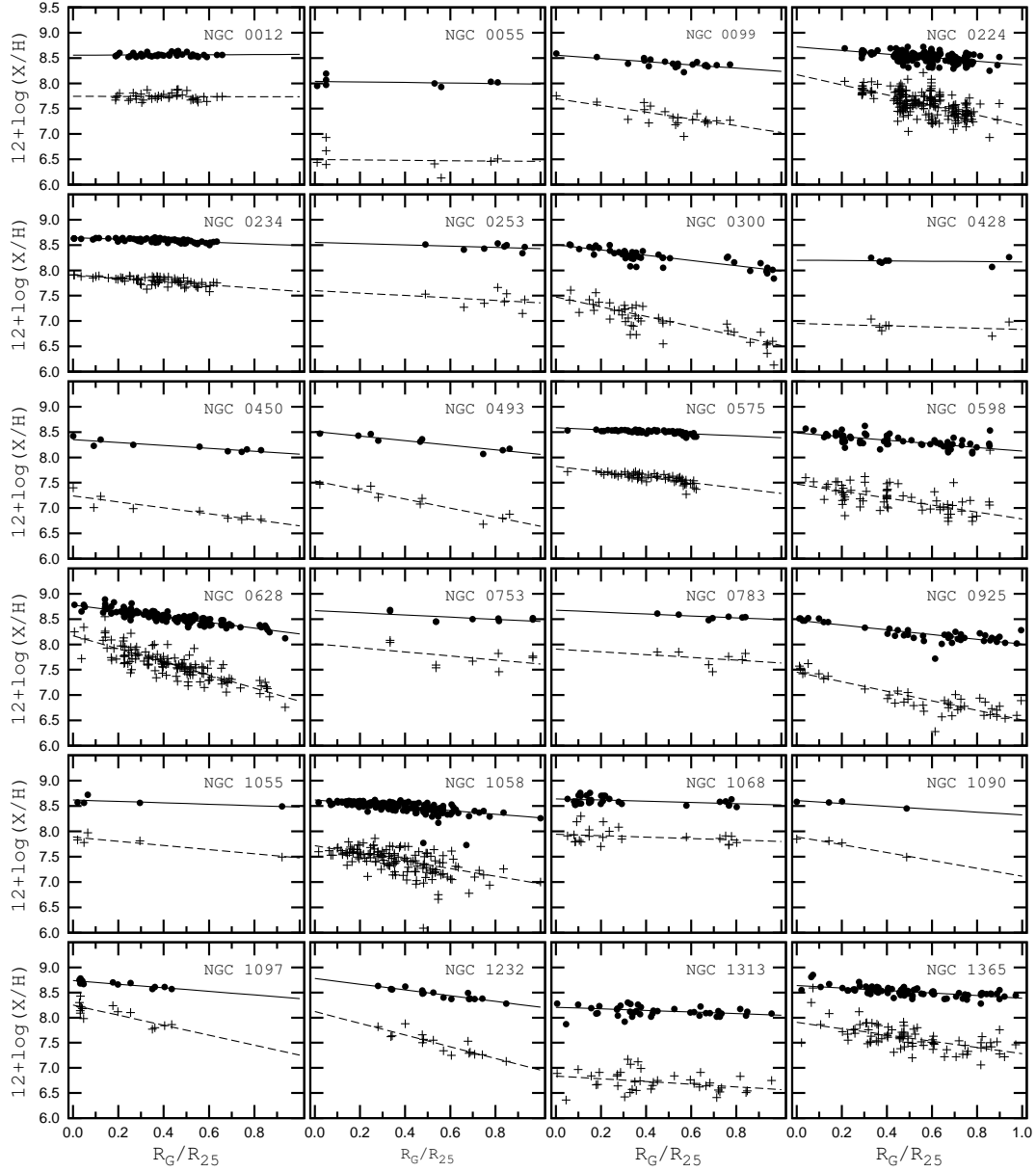


Fig. 1.— The radial distributions of the oxygen and nitrogen abundances in the disks of nearby galaxies. The oxygen abundances for individual H II regions are shown by the points. The linear best fits to the points are presented by solid lines. The galactocentric distances are normalized to the isophotal radius. The nitrogen abundances for individual H II regions are shown by the plus signs. The linear best fits to these latter data (plus signs) are given by dashed lines.

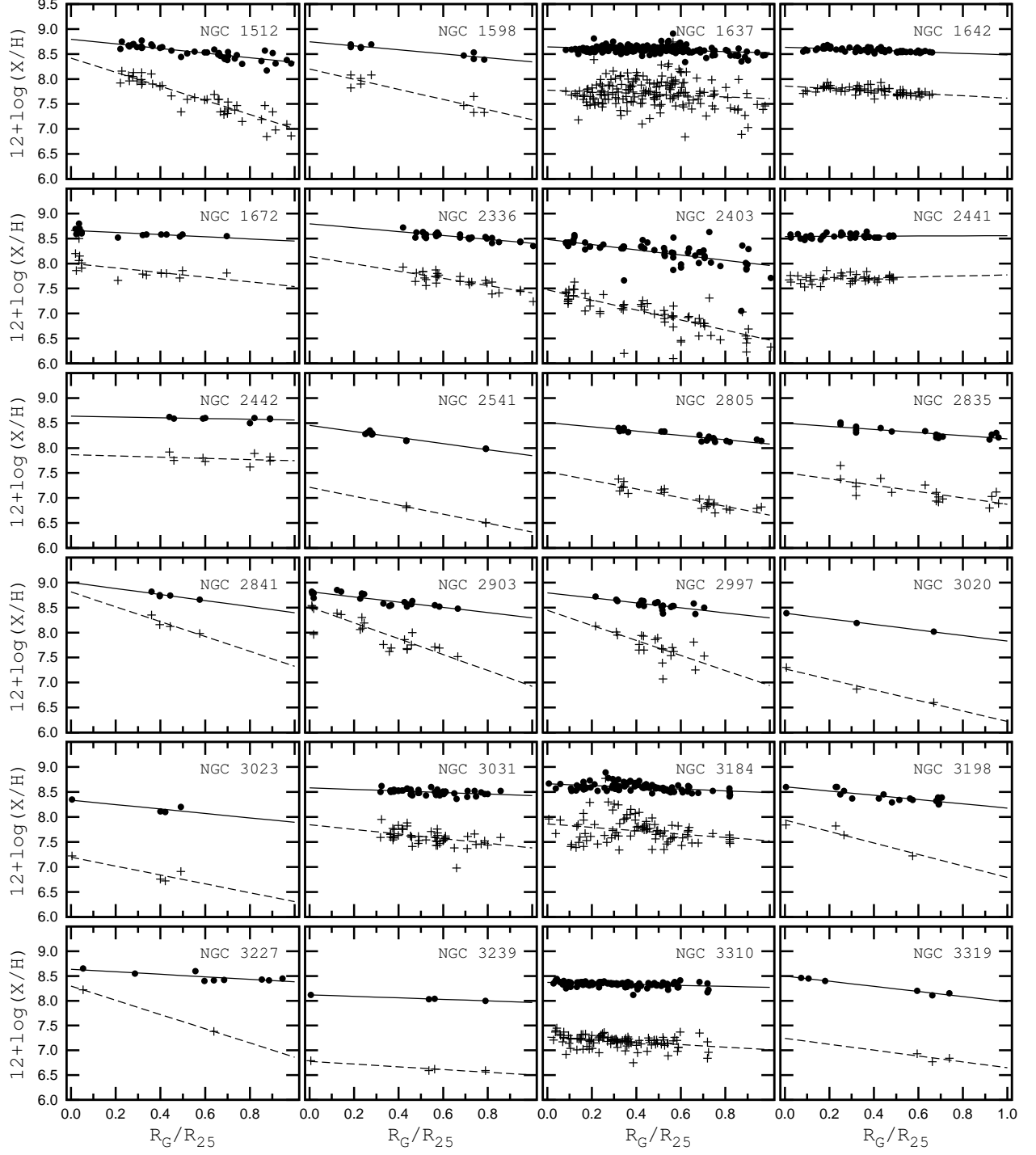


Fig. 1.— Continued

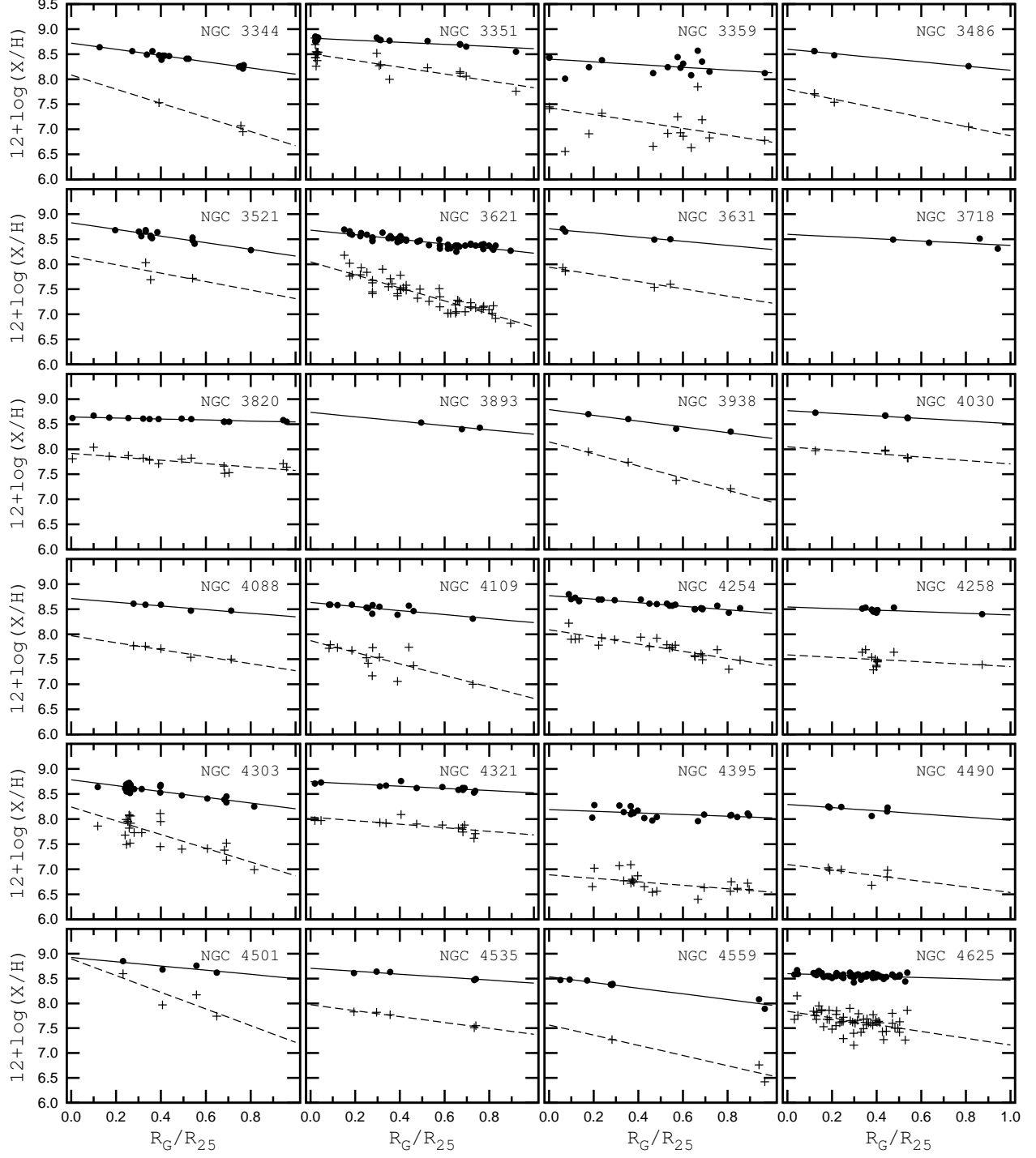


Fig. 1.— Continued



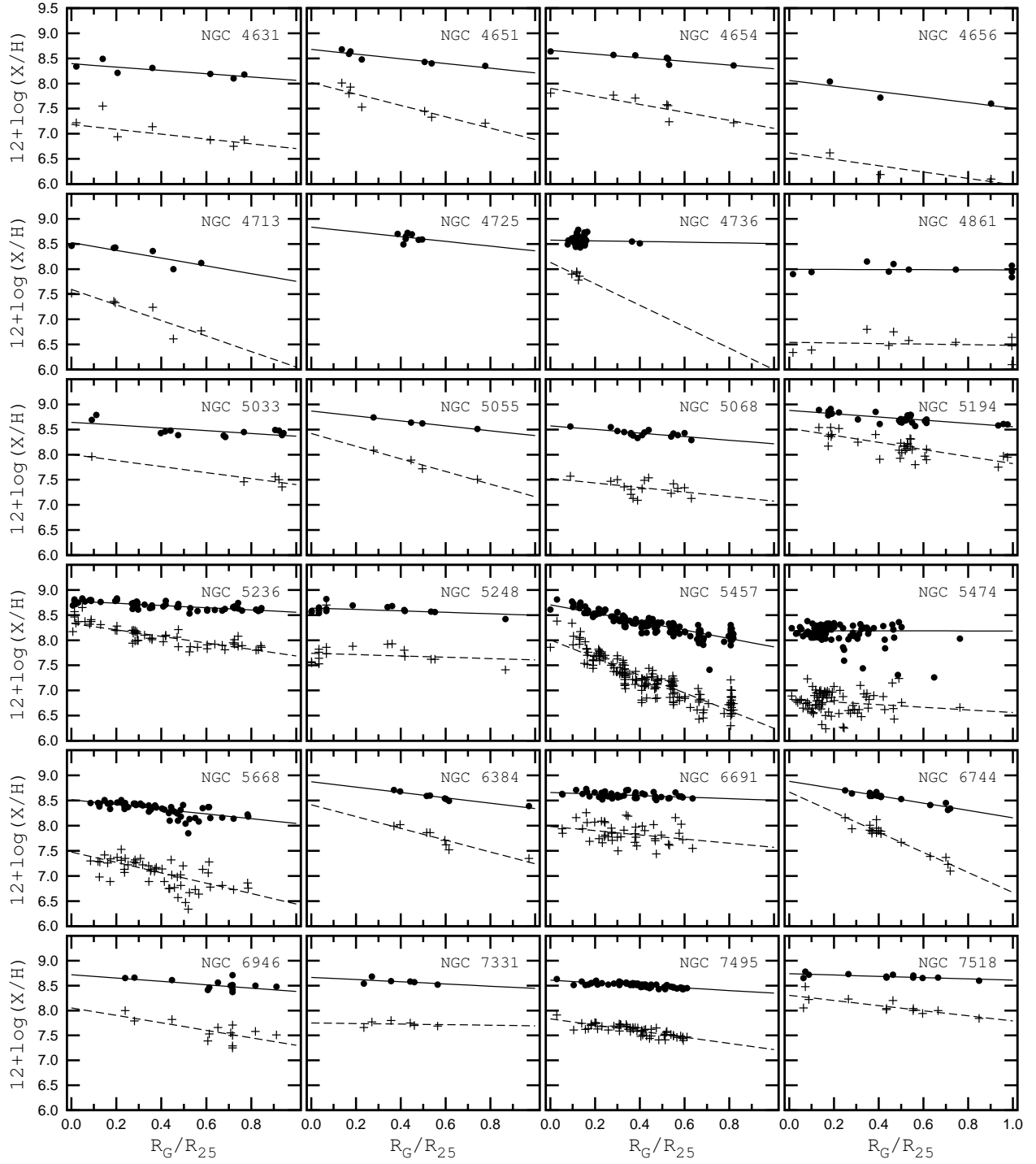


Fig. 1.— Continued

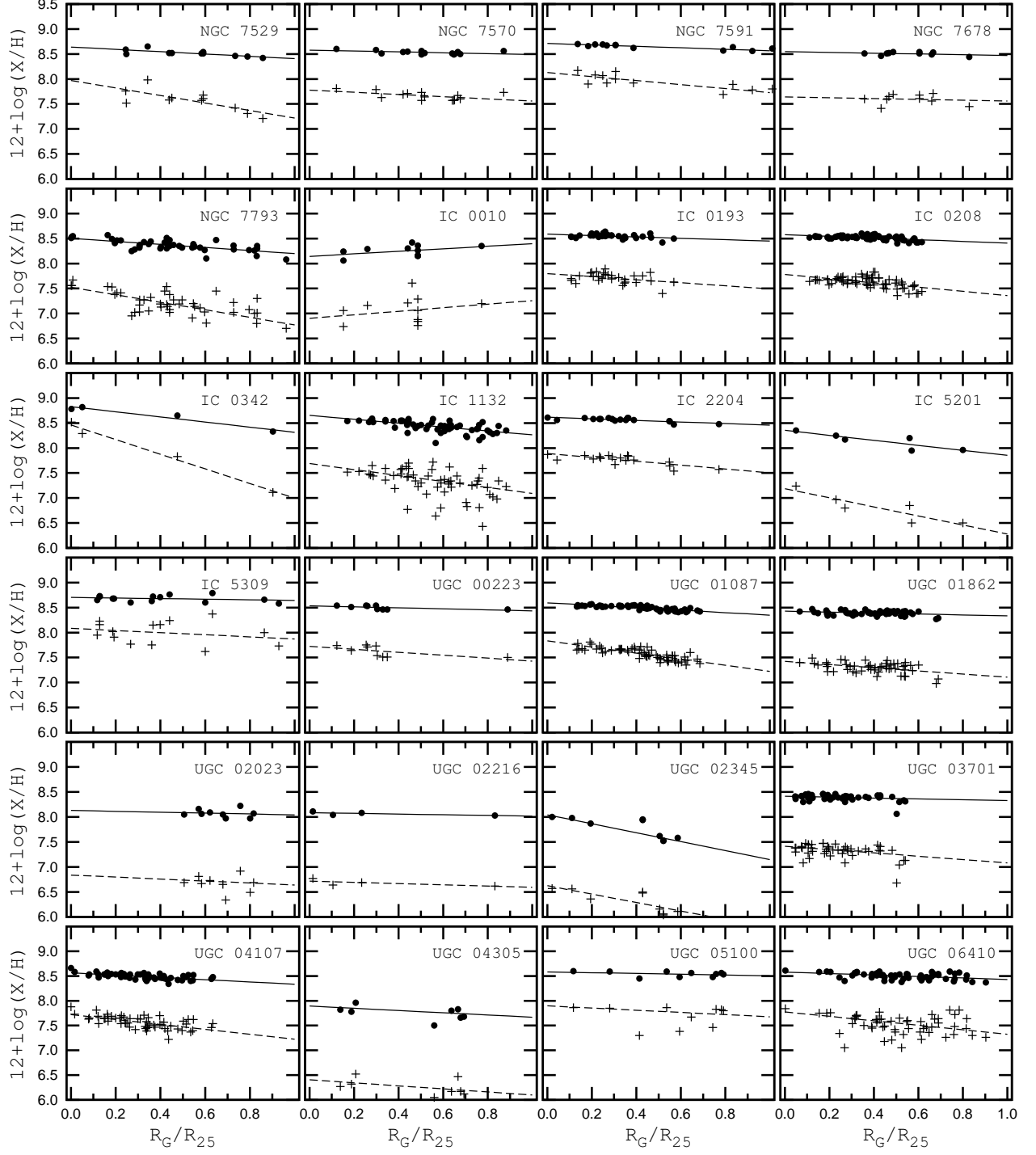


Fig. 1.— Continued

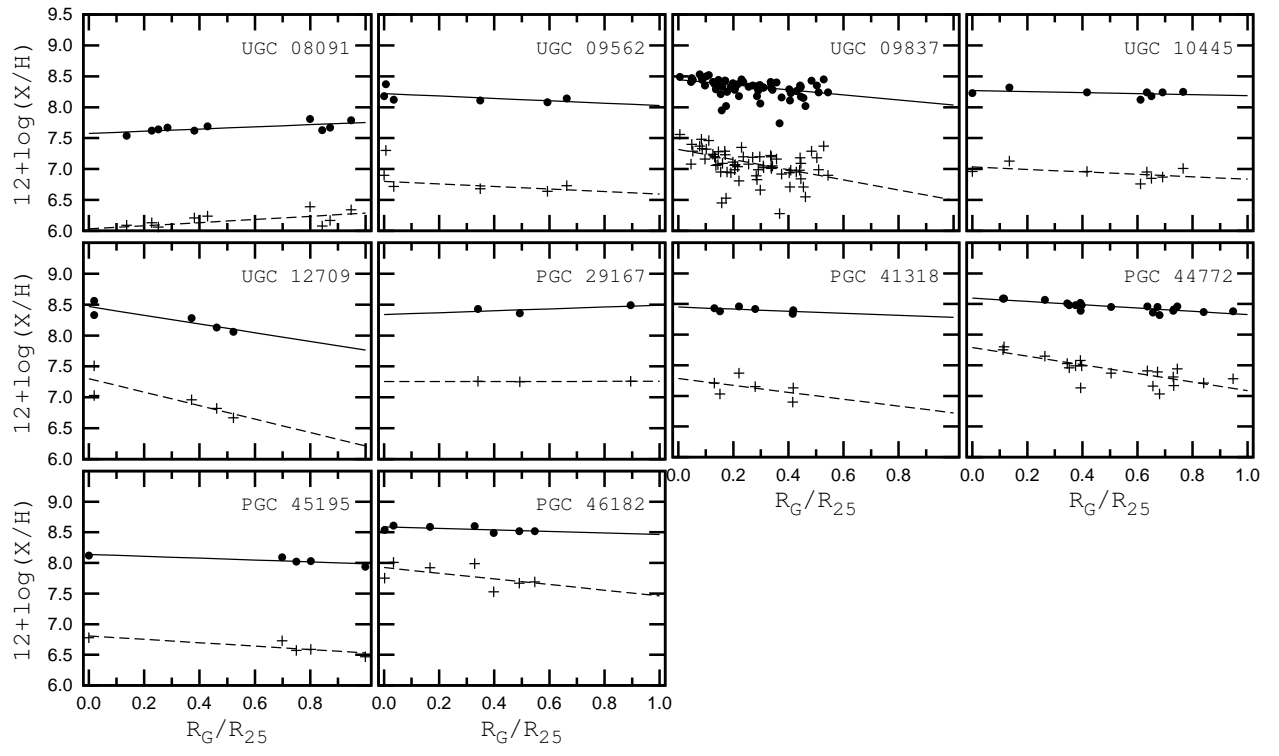


Fig. 1.— Continued

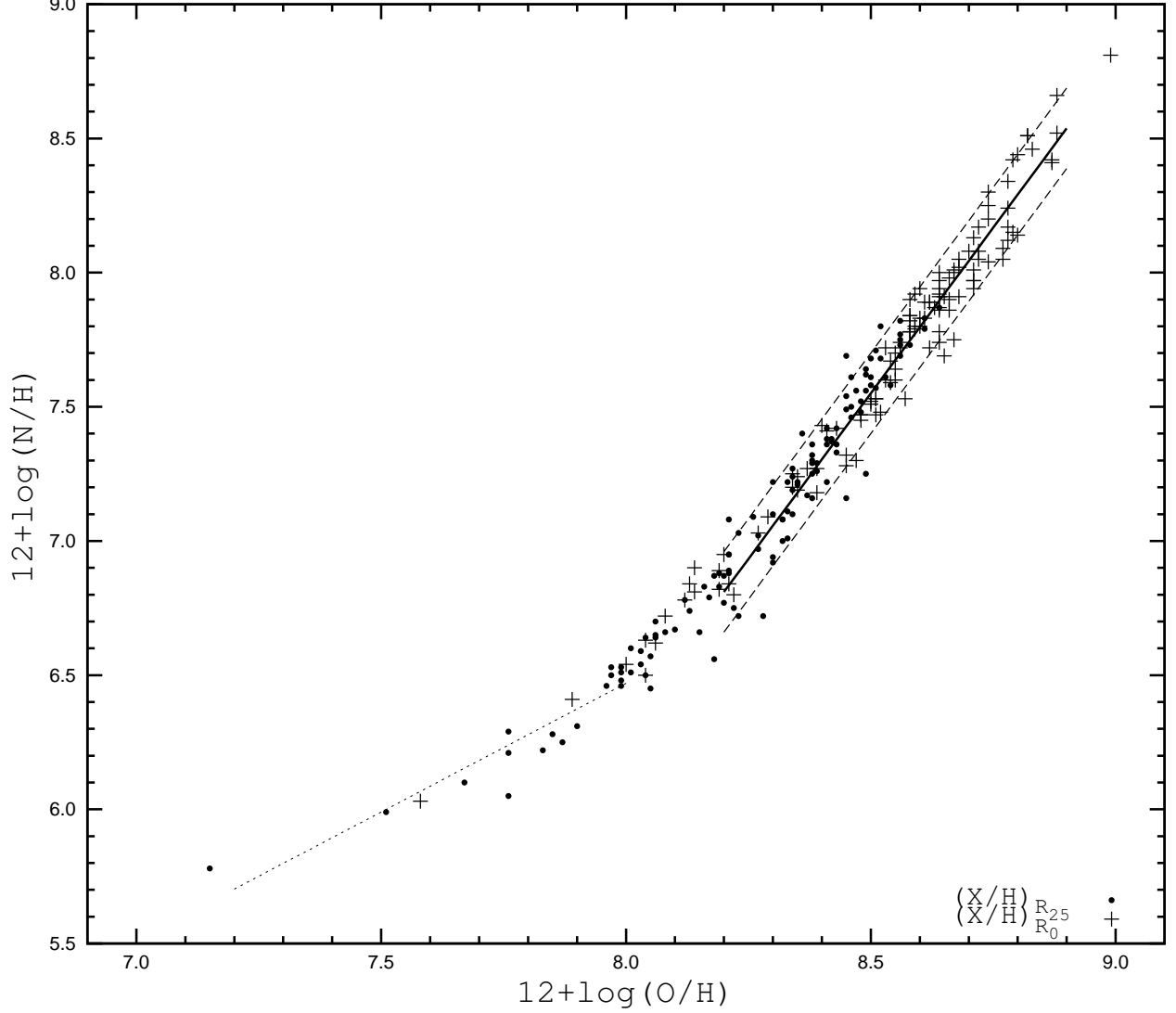


Fig. 2.— The N/H – O/H diagram. The plus signs are the central abundances. The points are abundances at the optical edges of a galaxy’s  $R_{25}$  isophotal radius. The solid line is the  $N/H = f(O/H)$  relation for central abundances at high metallicity, Eq. (7), the dashed lines are shifted along the Y-axis by  $\pm 0.15$  dex. The dotted line is the relation at low metallicity for both central abundances and abundances at the  $R_{25}$  radii of the galaxies.

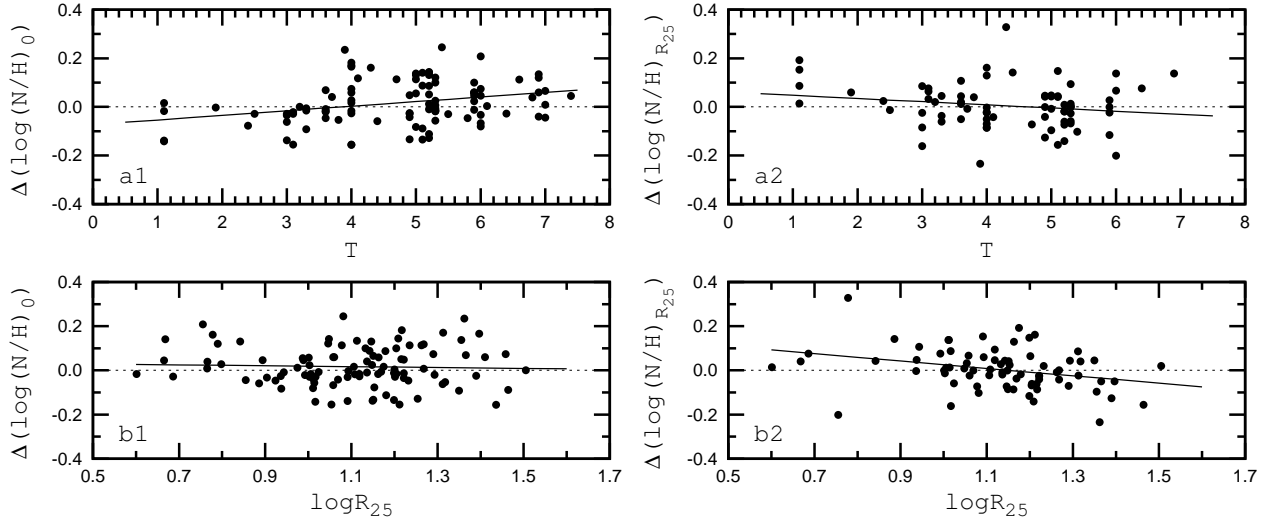


Fig. 3.— The residuals of Eq. (7) (panels *a1* and *b1*) and Eq. (8) (panels *a2* and *b2*) as a function of the morphological  $T$  type and linear radius of the galaxy  $R_{25}$ . The points show the values of the individual galaxies. The solid lines are linear best fits to those data. The dotted lines show zero-lines.

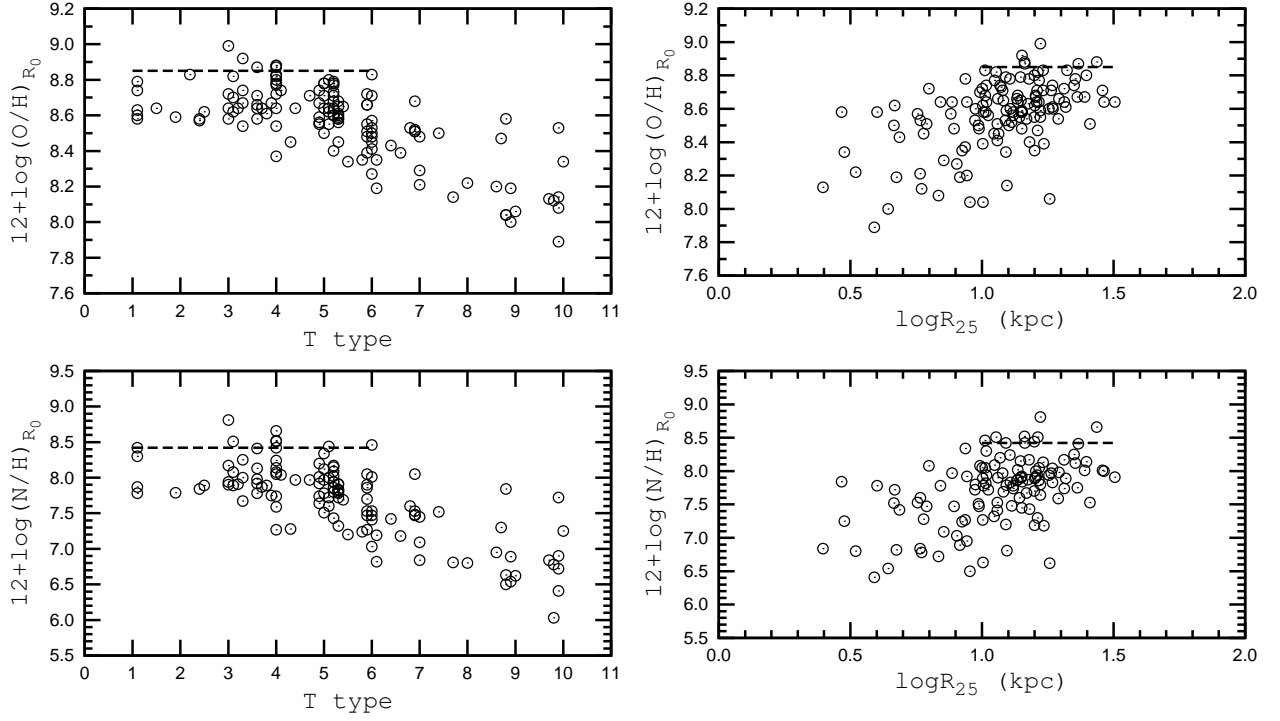


Fig. 4.— The central oxygen abundance,  $(\text{O}/\text{H})_{R_0}$ , and nitrogen abundance,  $(\text{N}/\text{H})_{R_0}$ , as a function of morphological  $T$  type (left panels) and of isophotal radius  $R_{25}$  of a galaxy (right panels). The dashed lines show the maximum oxygen and nitrogen abundances in the galaxies.

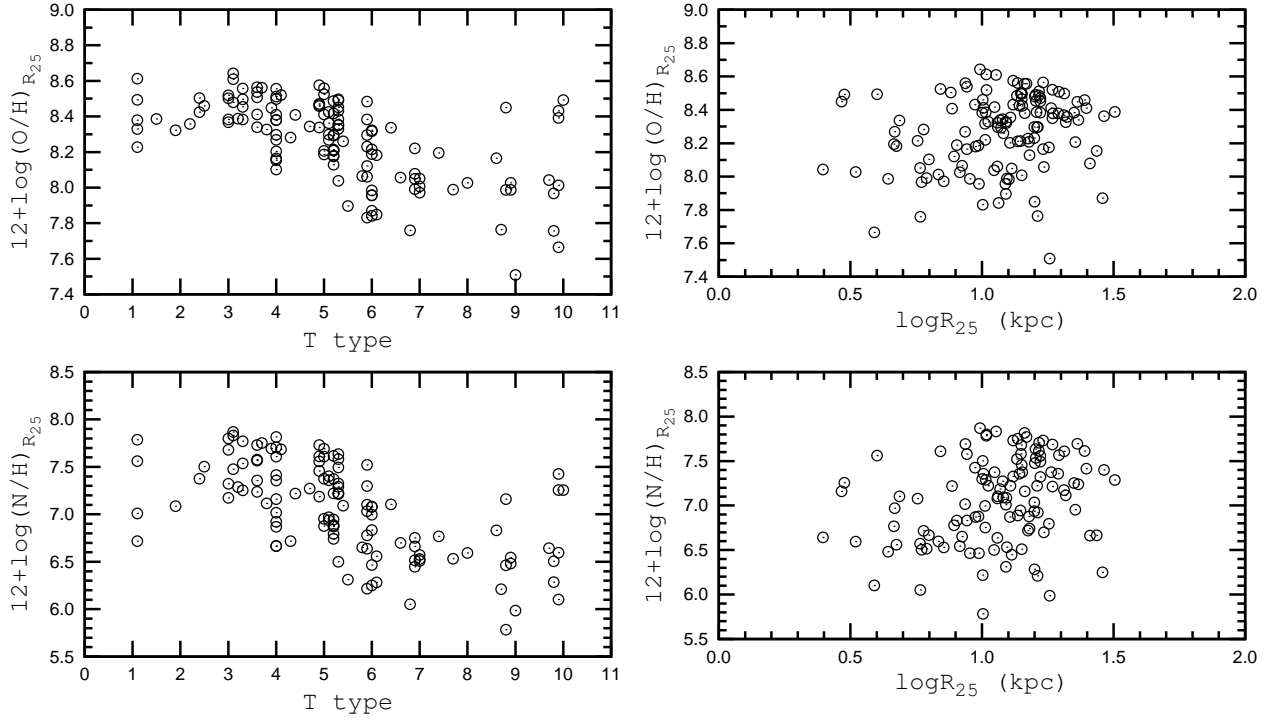


Fig. 5.— The oxygen abundances,  $(\text{O}/\text{H})_{R_{25}}$ , and nitrogen abundances,  $(\text{N}/\text{H})_{R_{25}}$ , measured at the  $R_{25}$  radius of the galaxies’ disks as a function of morphological  $T$  type (left panels) and of isophotal radius  $R_{25}$  of a given galaxy (right panels).

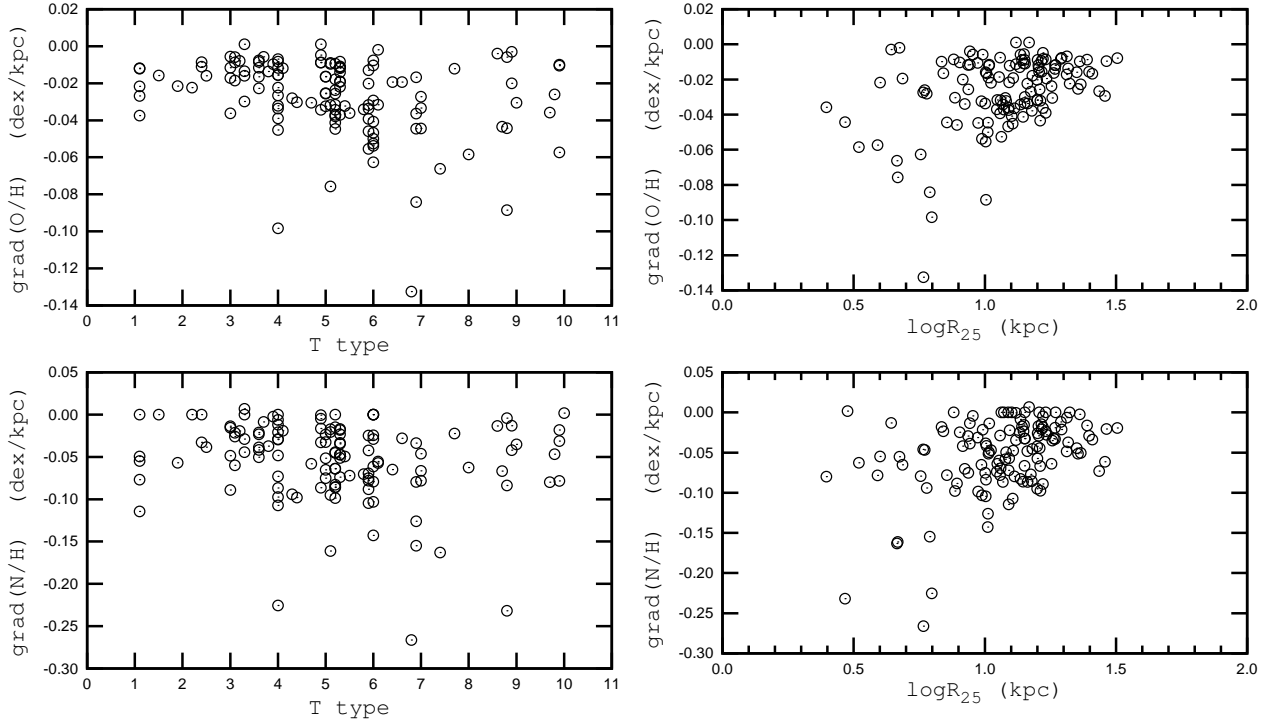


Fig. 6.— The radial oxygen and nitrogen abundance gradients in units of  $\text{dex kpc}^{-1}$  as a function of morphological  $T$  type (left panels) and of isophotal radius  $R_{25}$  of the galaxies (right panels).



Table 1. The adopted properties of our galaxies.

Galaxy	Type	T	R.A. degrees	Dec. degrees	$R_{25}$ arcmin	P.A. degrees	Inclination degrees	Reference	Distance Mpc	Reference	$R_{25}$ kpc
NGC 0012	Sc	4.9	2.486458	4.612528	0.85	125	27	1	53.20	2	13.14
NGC 0055	SBm	8.8	3.723333	-39.196639	16.18	110	79	3	1.91	4	8.99
NGC 0099	Sc	5.9	5.997470	15.770428	0.71	0	24	1	77.00	5	15.82
NGC 0224	Sb	3.0	10.684792	41.269065	95.27	35	77	6	0.74	7	20.51
NGC 0234	SABc	5.3	10.884977	14.342564	0.81	0	0	1	59.60	2	14.06
NGC 0253	SABc	5.1	11.888000	-25.288219	13.77	50	76	8	3.46	9	13.86
NGC 0300	Scd	6.9	13.722833	-37.684389	10.94	106	42	10	1.94	4	6.17
NGC 0428	SABm	8.6	18.232125	0.981557	2.04	120	41	1	14.80	11	8.77
NGC 0450	SABc	5.8	18.876840	-0.860974	1.54	72	41	1	18.70	11	8.40
NGC 0493	Sc	5.9	20.537458	0.945362	1.69	58	72	1	23.20	11	11.43
NGC 0575	Sc	5.3	22.694333	21.440417	0.85	0	21	1	41.80	2	10.32
NGC 0598	Sc	5.9	23.462042	30.660222	35.40	23	56	12	0.76	4	7.83
NGC 0628	Sc	5.2	24.173946	15.783661	5.24	25	6	13	9.91	14	15.09
NGC 0753	SABc	4.9	29.425833	35.916125	1.26	128	50	15	67.10	16	24.52
NGC 0783	Sc	5.3	30.277542	31.882472	0.79	35	27	1	69.30	2	15.98
NGC 0925	Scd	7.0	36.820333	33.579167	5.24	101	58	17	9.29	18	14.15
NGC 1055	SBb	3.1	40.438458	0.443168	3.79	105	69	1	14.40	11	15.89
NGC 1058	Sc	5.1	40.874988	37.341339	1.51	145	15	19	10.60	20	4.66
NGC 1068	Sb	3.0	40.669629	-0.013281	3.54	70	32	1	10.10	11	10.40
NGC 1090	Sbc	3.8	41.641401	-0.247158	1.99	102	64	1	35.90	16	20.79
NGC 1097	SBb	3.3	41.579375	-30.274889	4.67	134	46	21	16.50	2	22.40
NGC 1232	SABc	5.0	47.439625	-20.579306	3.71	90	30	22	21.00	2	22.64

Table 1—Continued

Galaxy	Type	T	R.A. degrees	Dec. degrees	$R_{25}$ arcmin	P.A. degrees	Inclination degrees	Reference	Distance Mpc	Reference	$R_{25}$ kpc
NGC 1313	SBcd	7.0	49.566875	-66.498250	4.56	4	38	23	4.39	24	5.82
NGC 1365	Sb	3.2	53.401546	-36.140403	5.61	42	46	25	19.60	18	32.00
NGC 1512	Sa	1.1	60.976167	-43.348861	4.46	80	35	26	9.50	27	12.32
NGC 1598	SBc	4.9	67.140292	-47.782556	0.72	123	55	1	55.80	16	11.73
NGC 1637	Sc	5.0	70.367408	-2.857961	1.99	31	40	19	12.00	18	6.95
NGC 1642	Sc	5.2	70.728792	0.618583	0.91	175	29	1	62.10	2	16.43
NGC 1672	Sb	3.3	71.427125	-59.247278	3.30	170	34	1	16.70	2	16.05
NGC 2336	Sbc	4.0	111.766875	80.178083	2.51 <sup>a</sup>	175	55	28	34.20	2	24.95
NGC 2403	SABc	6.0	114.214167	65.602556	10.94	126	58	29	3.06	18	9.74
NGC 2441	SABb	3.3	117.978083	73.015694	1.00	0	29	1	50.90	2	14.77
NGC 2442	Sbc	3.7	114.099333	-69.530833	2.75	27	29	30	17.10	31	13.67
NGC 2541	SABc	6.0	123.667148	49.061709	3.16	165	60	1	12.60	18	11.56
NGC 2805	SABc	6.9	140.085042	64.102778	3.16	125	41	1	28.00	31	25.70
NGC 2835	Sc	5.0	139.470458	-22.354667	3.30	160	45	32	10.10	16	9.71
NGC 2841	Sb	3.0	140.510975	50.976519	4.06	150	66	33	14.10	18	16.67
NGC 2903	SABb	4.0	143.042125	21.500833	6.30	22	65	34	8.90	35	16.30
NGC 2997	SABc	5.1	146.411625	-31.191083	4.46	107	32	36	12.20	36	15.82
NGC 3020	Sc	5.9	147.527500	12.813639	1.58	105	60	1	21.90	11	10.07
NGC 3023	SABc	5.5	147.469112	0.618167	1.44	70	60	1	29.40	2	12.33
NGC 3031	Sab	2.4	148.888221	69.065295	13.46	150	59	37	3.63	18	14.21
NGC 3184	SABc	5.9	154.570258	41.424053	3.71	135	21	1	12.60	14	13.59
NGC 3198	Sc	5.2	154.978966	45.549623	4.26	35	67	1	14.50	18	17.95

Table 1—Continued

Galaxy	Type	T	R.A. degrees	Dec. degrees	$R_{25}$ arcmin	P.A. degrees	Inclination degrees	Reference	Distance Mpc	Reference	$R_{25}$ kpc
NGC 3227	SABa	1.5	155.877412	19.865050	2.68	155	47	1	20.60	31	16.09
NGC 3239	IB	9.8	156.270375	17.163583	2.51	80	49	38	8.10	31	5.90
NGC 3310	SABb	4.0	159.691083	53.503383	1.54	163	39	39	19.20	2	8.63
NGC 3319	SBc	6.0	159.789414	41.686675	3.08	37	57	1	14.10	18	12.64
NGC 3344	Sbc	4.0	160.879792	24.922222	3.54	156	25	40	6.10	31	6.28
NGC 3351	Sb	3.1	160.990417	11.703806	3.71	13	42	26	10.50	18	11.32
NGC 3359	Sc	5.2	161.653596	63.224236	3.62	172	51	41	14.40	42	15.17
NGC 3486	Sc	5.2	165.099452	28.975137	3.54	80	42	1	9.16	2	9.43
NGC 3521	SABb	4.0	166.452421	-0.035864	5.48	160	73	37	10.70	43	17.06
NGC 3621	SBcd	6.9	169.568792	-32.814056	4.89 <sup>b</sup>	165	65	37	7.24	18	10.29
NGC 3631	Sc	5.2	170.261976	53.169569	2.51	152	20	86	22.2	2	16.18
NGC 3718	Sa	1.1	173.145221	53.067922	3.77 <sup>c</sup>	15	65	44	17.00	31	18.63
NGC 3820	Sbc	3.6	175.520442	10.384253	0.33	26	42	45	91.30	2	8.77
NGC 3893	SABc	5.2	177.159125	48.710833	2.23	165	52	1	18.20	11	11.82
NGC 3938	Sc	5.2	178.206042	44.120722	2.68	15	24	1	17.90	46	13.98
NGC 4030	Sbc	4.0	180.098445	-1.100095	2.08	27	44	1	27.20	11	16.49
NGC 4088	SABc	4.7	181.392458	50.539028	2.88	43	67	1	14.30	11	11.97
NGC 4109	Sa	1.1	181.713008	42.995642	0.50	147	44	45	102.80	2	14.95
NGC 4254	Sc	5.2	184.706683	14.416508	2.68	59	29	19	14.30	16	11.17
NGC 4258	SABb	4.0	184.739600	47.303972	9.31	150	72	47	7.20	48	19.50
NGC 4303	Sbc	4.0	185.478729	4.473647	3.23	137	27	19	13.60	2	12.77
NGC 4321	SABb	4.1	185.728462	15.821817	3.71	30	32	1	17.20	18	18.55

Table 1—Continued

Galaxy	Type	T	R.A. degrees	Dec. degrees	$R_{25}$ arcmin	P.A. degrees	Inclination degrees	Reference	Distance Mpc	Reference	$R_{25}$ kpc
NGC 4395	Sm	8.9	186.453592	33.546928	6.59	147	46	49	4.30	50	8.24
NGC 4490	SBcd	7.0	187.650996	41.643898	3.16	125	61	1	7.80	31	7.16
NGC 4501	Sb	3.3	187.996503	14.420387	3.46	141	63	51	14.10	52	14.19
NGC 4535	Sc	5.0	188.584625	8.197750	3.54	0	45	1	17.80	18	18.33
NGC 4559	Sc	6.0	188.990195	27.959992	5.36	143	67	53	7.87	16	12.27
NGC 4625	SABm	8.8	190.469671	41.273964	1.09	130	27	54	9.20	18	2.93
NGC 4631	SBcd	6.6	190.533375	32.541500	7.74	86	80	1	7.62	55	17.17
NGC 4651	Sc	5.2	190.927625	16.393389	1.99	78	48	19	23.60	56	13.67
NGC 4654	Sc	5.9	190.985750	13.126681	2.45	122	57	19	16.10	16	11.47
NGC 4656	SBm	9.0	190.990531	32.168150	7.57	33	79	1	8.20	2	18.05
NGC 4713	Scd	6.8	192.491139	5.311405	1.35	50	35	57	14.90	11	5.83
NGC 4725	SABa	2.2	192.610755	25.500805	5.36	35	45	1	13.50	18	21.04
NGC 4736	Sab	2.4	192.721088	41.120458	5.61	116	37	58	4.66	24	7.60
NGC 4861	Sm	8.9	194.759754	34.859444	1.99	23	69	59	7.59	11	4.40
NGC 5033	Sc	5.1	198.364441	36.569936	5.36	170	62	1	18.70	16	29.14
NGC 5055	Sbc	4.0	198.955542	42.029278	6.30	101	64	33	7.94	11	14.54
NGC 5068	Sc	6.0	199.728375	-21.039111	3.62	110	29	1	5.40	60	5.69
NGC 5194	Sbc	4.0	202.469629	47.195172	5.61	163	52	1	8.90	61	14.52
NGC 5236	Sc	5.0	204.253958	-29.865417	6.44	46	24	58	4.61	18	8.64
NGC 5248	SABb	4.0	204.383433	8.885178	3.08	110	44	1	22.90	2	20.54
NGC 5457	SABc	6.0	210.802267	54.348950	14.42	37	18	62	6.85	18	28.73
NGC 5474	Sc	6.1	211.256708	53.662222	2.39	159	21	63	6.80	35	4.73

Table 1—Continued

Galaxy	Type	T	R.A. degrees	Dec. degrees	$R_{25}$ arcmin	P.A. degrees	Inclination degrees	Reference	Distance Mpc	Reference	$R_{25}$ kpc
NGC 5668	Scd	6.9	218.351408	4.450458	1.66	164	21	64	26.90	31	12.96
NGC 6384	SABb	3.6	263.101250	7.060278	3.08	32	48	19	25.90	11	23.23
NGC 6691	Sbc	3.6	279.801042	55.641806	0.79	0	21	1	85.10	2	19.62
NGC 6744	Sbc	4.0	287.442125	-63.857528	9.98	20	50	65	9.40	16	27.28
NGC 6946	SABc	5.9	308.718012	60.153914	5.74	62	38	66	6.00	67	10.02
NGC 7331	Sbc	3.9	339.266725	34.415519	5.24	169	75	28	15.10	68	23.00
NGC 7495	SABc	5.3	347.238250	12.048028	0.91	5	24	1	70.00	69	18.53
NGC 7518	SABa	1.1	348.303042	6.321667	0.71	109	42	70	50.50	70	10.38
NGC 7529	Sbc	4.4	348.513292	8.992500	0.43	0	17	1	62.10	2	7.69
NGC 7570	Sa	1.1	349.186134	13.483011	0.77	30	54	1	17.70	16	3.99
NGC 7591	SBbc	3.6	349.567833	6.585806	0.98	148	68	71	60.20	16	17.07
NGC 7678	Sc	4.9	352.116250	22.421194	1.17	5	45	1	48.90	2	16.67
NGC 7793	Scd	7.4	359.457625	-32.591028	4.67	99	54	10	3.40	72	4.62
IC 0010	IB	9.9	5.072250	59.303778	3.16	125	27	45	0.66	73	0.61
IC 0193	Sc	5.3	30.629083	11.093083	0.93	154	32	1	61.60	2	16.68
IC 0208	Sbc	3.6	32.115583	6.394917	0.91	0	12	1	38.30	16	10.14
IC 0342	SABc	6.0	56.702096	68.096367	10.69	37	31	74	3.30	68	10.26
IC 1132	Sc	5.4	235.028171	20.680606	0.59	50	18	75	70.60	2	12.06
IC 2204	Sab	2.5	115.325435	34.232169	0.52	0	0	1	66.20	76	10.08
IC 5201	Sc	6.1	335.239333	-46.035861	4.26	33	63	1	12.80	2	15.85
IC 5309	Sb	3.1	349.798542	8.109306	0.67	20	63	77	50.00	16	9.81
UGC 00223	I	9.9	6.177915	14.824582	0.46	0	0	1	70.80	2	9.39

Table 1—Continued

Galaxy	Type	T	R.A. degrees	Dec. degrees	$R_{25}$ arcmin	P.A. degrees	Inclination degrees	Reference	Distance Mpc	Reference	$R_{25}$ kpc
UGC 01087	Sc	5.3	22.860833	14.277500	0.74	0	21	1	59.60	2	12.82
UGC 01862	SABc	6.4	36.103375	-2.162361	0.83	10	39	1	20.10	16	4.85
UGC 02023	I	9.7	37.572417	33.491111	0.83	59	26	78	10.30	79	2.49
UGC 02216	I	9.9	41.087913	0.675381	0.64	15	72	1	36.50	2	6.84
UGC 02345	Sm	8.8	42.969583	-1.172222	1.73	160	30	1	20.00	2	10.09
UGC 03701	Sc	6.0	107.927833	72.169306	0.91	0	0	1	43.20	2	11.43
UGC 04107	Sc	5.3	119.257792	49.567361	0.71	0	12	1	51.50	2	10.58
UGC 04305	I	9.9	124.770750	70.720027	3.97	177	40	80	3.38	9	3.90
UGC 05100	SBb	3.0	143.661008	5.841439	0.60	30	53	1	80.60	2	14.09
UGC 06410	SABc	5.3	171.024500	45.811072	0.55	5	39	1	82.50	2	13.16
UGC 08091	I	9.8	194.668512	14.217511	0.54	170	20	81	2.08	9	0.32
UGC 09562	Sd	8.0	222.810048	35.542269	0.48	30	27	1	23.80	31	3.31
UGC 09837	SABc	5.3	230.965311	58.052941	0.91	21	18	82	42.00	82	11.12
UGC 10445	Sc	6.0	248.448417	28.984778	1.38	142	46	83	20.00	2	8.01
UGC 12709	SABm	8.7	354.350001	0.391670	1.51	145	47	1	37.00	2	16.25
PGC 29167	I	10.0	150.965417	68.690278	2.70 <sup>d</sup>	0	0		3.82	84	3.00
PGC 41318	S?	4.3	187.589848	56.791542	0.29	0	21	45	70.10	2	6.00
PGC 44772	S?	1.9	195.138542	10.129969	0.40	128	32	45	107.80	2	12.39
PGC 45195	Sd	7.7	196.129979	-3.572419	1.77	63	44	1	24.10	2	12.44
PGC 46182	Sc	4.9	199.061225	41.494460	0.54 <sup>e</sup>	34	52	85	89.40	76	14.15

<sup>a</sup>from Gusev et al. (2012)

<sup>b</sup>from Bresolin et al. (2012)

<sup>c</sup>from Tully et al. (1996)

<sup>d</sup>from Croxall et al. (2009)

<sup>e</sup>from Petrosian et al. (2007)

References. — (1) – de Vaucouleurs et al. (1991) (RC3); (2) – NED; (3) – Puche et al. (1991); (4) – Bono et al. (2010); (5) – Gil de Paz et al. (2007); (6) – Walterbos & Kennicutt (1987); (7) – Vilardell et al. (2010); (8) – Hlavacek-Larrondo et al. (2011); (9) – Dalcanton et al. (2009); (10) – Carignan (1985); (11) – Tully et al. (2009); (12) – Zaritsky et al. (1989); (13) – Kamphuis & Briggs (1992); (14) – Olivares et al. (2010); (15) – Amram et al. (1994); (16) – Springob et al. (2009); (17) – Pisano et al. (1998); (18) – Saha et al. (2006); (19) – García-Gómez et al. (2004); (20) – Schmidt et al. (1994); (21) – Ondrechen et al. (1989); (22) – van Zee & Bryant (1999); (23) – Marcelin & Athanassoula (1982); (24) – Jacobs et al. (2009); (25) – Ondrechen & van der Hulst (1989); (26) – Dicaire et al. (2008); (27) – Bresolin et al. (2012); (28) – Gusev et al. (2012); (29) – Zaritsky et al. (1990); (30) – Riad et al. (2010); (31) – Tully (1988); (32) – Kirby et al. (2008); (33) – Blais-Ouellette et al. (2004); (34) – Marcelin et al. (1983); (35) – Drozdovsky & Karrachentsev (2000); (36) – Hess et al. (2009); (37) – de Blok et al. (2008); (38) – Lee et al. (2011); (39) – Rosales-Ortega et al. (2010); (40) – Verdes-Montenegro et al. (2000); (41) – Ball (1986); (42) – Zahid & Bresolin (2011); (43) – Walter et al. (2008); (44) – Tully et al. (1996); (45) – Paturel et al. (2003) (LEDA); (46) – Poznanski et al. (2009); (47) – van Albada (1980); (48) – Humphreys et al. (2008); (49) – de Blok & Bosma (2002); (50) – Thim et al. (2004); (51) – Send (1982); (52) – Wood-Vasey et al. (2008); (53) – Barbieri et al. (2005); (54) – Bush & Wilcots (2004); (55) – Seth et al. (2005); (56) – Terry et al. (2002); (57) – Moustakas & Kennicutt (2006b); (58) – Herrmann & Ciardullo (2009); (59) – Swaters & Balcells (2002); (60) – Herrmann et al. (2008); (61) – Dessart et al. (2008); (62) – Kamphuis (1993); (63) – Rownd et al. (1994); (64) – Grosbøl (1985); (65) – Whiteoak & Gardner (1977); (66) – Boomsma et al. (2008); (67) – Sharina et al. (1997); (68) – Saha et al. (2002); (69) – Müller & Höflich (1994); (70) – Moustakas & Kennicutt (2006a); (71) – Rubin et al. (1988); (72) – Pietrzyński et al. (2010); (73) – Sakai et al. (1999); (74) – Crosthwaite et al. (2000); (75) – Peletier et al. (1999); (76) – Kopparapu et al. (2008); (77) – Amram et al. (1992); (78) – van Zee (2000); (79) – Tikhonov & Galazoutdinova (2002); (80) – Puche et al. (1992); (81) – Begum & Chengalur (2003); (82) – Pohlen & Trujillo (2006); (83) – Epinat et al. (2008); (84) – Karachentsev et al. (2002); (85) – Petrosian et al. (2007); (86) – Barberá et al. (2004)

Table 2. The derived parameters of the radial oxygen and nitrogen abundance distributions in galaxies.

Galaxy	$12+\log(\text{O}/\text{H})_{R_0}$	O/H gradient dex $R_{25}^{-1}$	O/H gradient dex $\text{kpc}^{-1}$	$\sigma(\text{O}/\text{H})$ dex	$12+\log(\text{N}/\text{H})_{R_0}$	N/H gradient dex $R_{25}^{-1}$	N/H gradient dex $\text{kpc}^{-1}$	$\sigma(\text{N}/\text{H})$ dex
NGC 0012	$8.56 \pm 0.02$	$0.015 \pm 0.042$	$0.0011 \pm 0.0032$	0.033	$7.74 \pm 0.04$	$-0.008 \pm 0.087$	$-0.0006 \pm 0.0066$	0.068
NGC 0055	$8.04 \pm 0.05$	$-0.053 \pm 0.094$	$-0.0059 \pm 0.0104$	0.075	$6.50 \pm 0.07$	$-0.037 \pm 0.131$	$-0.0042 \pm 0.0145$	0.091
NGC 0099	$8.55 \pm 0.04$	$-0.319 \pm 0.072$	$-0.0202 \pm 0.0045$	0.055	$7.70 \pm 0.07$	$-0.666 \pm 0.137$	$-0.0422 \pm 0.0087$	0.105
NGC 0224	$8.72 \pm 0.02$	$-0.352 \pm 0.039$	$-0.0172 \pm 0.0019$	0.077	$8.17 \pm 0.04$	$-0.996 \pm 0.072$	$-0.0486 \pm 0.0035$	0.136
NGC 0234	$8.65 \pm 0.01$	$-0.154 \pm 0.022$	$-0.0109 \pm 0.0015$	0.027	$7.91 \pm 0.02$	$-0.329 \pm 0.046$	$-0.0234 \pm 0.0033$	0.058
NGC 0253	$8.55 \pm 0.13$	$-0.125 \pm 0.164$	$-0.0090 \pm 0.0119$	0.055	$7.60 \pm 0.35$	$-0.241 \pm 0.441$	$-0.0174 \pm 0.0319$	0.149
NGC 0300	$8.51 \pm 0.02$	$-0.519 \pm 0.040$	$-0.0842 \pm 0.0065$	0.069	$7.47 \pm 0.04$	$-0.955 \pm 0.080$	$-0.1548 \pm 0.0129$	0.130
NGC 0428	$8.20 \pm 0.06$	$-0.035 \pm 0.109$	$-0.0040 \pm 0.0124$	0.059	$6.95 \pm 0.11$	$-0.118 \pm 0.184$	$-0.0135 \pm 0.0210$	0.099
NGC 0450	$8.35 \pm 0.03$	$-0.285 \pm 0.057$	$-0.0340 \pm 0.0067$	0.046	$7.24 \pm 0.06$	$-0.589 \pm 0.112$	$-0.0702 \pm 0.0133$	0.092
NGC 0493	$8.51 \pm 0.04$	$-0.450 \pm 0.070$	$-0.0393 \pm 0.0061$	0.053	$7.53 \pm 0.07$	$-0.893 \pm 0.124$	$-0.0780 \pm 0.0109$	0.093
NGC 0575	$8.58 \pm 0.01$	$-0.195 \pm 0.026$	$-0.0189 \pm 0.0025$	0.026	$7.82 \pm 0.03$	$-0.530 \pm 0.061$	$-0.0514 \pm 0.0059$	0.060
NGC 0598	$8.48 \pm 0.02$	$-0.359 \pm 0.041$	$-0.0459 \pm 0.0053$	0.073	$7.47 \pm 0.04$	$-0.691 \pm 0.084$	$-0.0883 \pm 0.0107$	0.145
NGC 0628	$8.78 \pm 0.01$	$-0.572 \pm 0.027$	$-0.0379 \pm 0.0018$	0.060	$8.17 \pm 0.03$	$-1.292 \pm 0.064$	$-0.0856 \pm 0.0042$	0.137
NGC 0753	$8.67 \pm 0.08$	$-0.212 \pm 0.106$	$-0.0087 \pm 0.0043$	0.065	$8.01 \pm 0.20$	$-0.399 \pm 0.290$	$-0.0163 \pm 0.0118$	0.177
NGC 0783	$8.68 \pm 0.07$	$-0.189 \pm 0.104$	$-0.0118 \pm 0.0056$	0.031	$7.91 \pm 0.30$	$-0.274 \pm 0.434$	$-0.0171 \pm 0.0272$	0.130
NGC 0925	$8.48 \pm 0.02$	$-0.473 \pm 0.037$	$-0.0334 \pm 0.0026$	0.067	$7.45 \pm 0.04$	$-0.941 \pm 0.071$	$-0.0665 \pm 0.0050$	0.128
NGC 1055	$8.62 \pm 0.04$	$-0.140 \pm 0.100$	$-0.0088 \pm 0.0063$	0.059	$7.89 \pm 0.05$	$-0.414 \pm 0.118$	$-0.0261 \pm 0.0074$	0.070
NGC 1058	$8.62 \pm 0.01$	$-0.352 \pm 0.027$	$-0.0757 \pm 0.0058$	0.055	$7.72 \pm 0.03$	$-0.751 \pm 0.069$	$-0.1613 \pm 0.0149$	0.137
NGC 1068	$8.64 \pm 0.02$	$-0.121 \pm 0.051$	$-0.0116 \pm 0.0049$	0.070	$7.94 \pm 0.04$	$-0.141 \pm 0.100$	$-0.0136 \pm 0.0096$	0.126
NGC 1090	$8.61 \pm 0.03$	$-0.284 \pm 0.103$	$-0.0137 \pm 0.0050$	0.026	$7.89 \pm 0.04$	$-0.775 \pm 0.131$	$-0.0373 \pm 0.0063$	0.033
NGC 1097	$8.74 \pm 0.01$	$-0.357 \pm 0.054$	$-0.0159 \pm 0.0024$	0.030	$8.25 \pm 0.05$	$-0.997 \pm 0.209$	$-0.0445 \pm 0.0093$	0.114
NGC 1232	$8.78 \pm 0.04$	$-0.573 \pm 0.068$	$-0.0253 \pm 0.0030$	0.040	$8.12 \pm 0.10$	$-1.166 \pm 0.172$	$-0.0515 \pm 0.0076$	0.103



Table 2—Continued

Galaxy	$12+\log(\text{O}/\text{H})_{R_0}$	O/H gradient dex $R_{25}^{-1}$	O/H gradient dex $\text{kpc}^{-1}$	$\sigma(\text{O}/\text{H})$ dex	$12+\log(\text{N}/\text{H})_{R_0}$	N/H gradient dex $R_{25}^{-1}$	N/H gradient dex $\text{kpc}^{-1}$	$\sigma(\text{N}/\text{H})$ dex
NGC 1313	$8.21 \pm 0.03$	$-0.159 \pm 0.051$	$-0.0273 \pm 0.0087$	0.071	$6.84 \pm 0.05$	$-0.269 \pm 0.096$	$-0.0462 \pm 0.0165$	0.132
NGC 1365	$8.64 \pm 0.02$	$-0.253 \pm 0.033$	$-0.0079 \pm 0.0010$	0.064	$7.91 \pm 0.04$	$-0.622 \pm 0.080$	$-0.0193 \pm 0.0024$	0.137
NGC 1512	$8.79 \pm 0.03$	$-0.461 \pm 0.048$	$-0.0374 \pm 0.0039$	0.066	$8.42 \pm 0.05$	$-1.410 \pm 0.083$	$-0.1144 \pm 0.0067$	0.115
NGC 1598	$8.74 \pm 0.03$	$-0.402 \pm 0.062$	$-0.0343 \pm 0.0053$	0.042	$8.20 \pm 0.09$	$-1.014 \pm 0.178$	$-0.0865 \pm 0.0152$	0.122
NGC 1637	$8.64 \pm 0.01$	$-0.115 \pm 0.023$	$-0.0165 \pm 0.0034$	0.062	$7.78 \pm 0.03$	$-0.170 \pm 0.067$	$-0.0236 \pm 0.0096$	0.160
NGC 1642	$8.64 \pm 0.01$	$-0.154 \pm 0.024$	$-0.0094 \pm 0.0015$	0.030	$7.86 \pm 0.02$	$-0.244 \pm 0.050$	$-0.0148 \pm 0.0031$	0.062
NGC 1672	$8.67 \pm 0.02$	$-0.216 \pm 0.070$	$-0.0135 \pm 0.0044$	0.055	$8.00 \pm 0.05$	$-0.464 \pm 0.158$	$-0.0290 \pm 0.0098$	0.119
NGC 2336	$8.80 \pm 0.04$	$-0.390 \pm 0.056$	$-0.0156 \pm 0.0022$	0.041	$8.14 \pm 0.08$	$-0.725 \pm 0.121$	$-0.0290 \pm 0.0049$	0.088
NGC 2403	$8.48 \pm 0.02$	$-0.524 \pm 0.043$	$-0.0538 \pm 0.0044$	0.079	$7.47 \pm 0.03$	$-1.005 \pm 0.069$	$-0.1032 \pm 0.0071$	0.128
NGC 2441	$8.54 \pm 0.01$	$0.017 \pm 0.040$	$0.0011 \pm 0.0027$	0.036	$7.67 \pm 0.03$	$0.100 \pm 0.080$	$0.0068 \pm 0.0054$	0.072
NGC 2442	$8.64 \pm 0.05$	$-0.079 \pm 0.072$	$-0.0058 \pm 0.0052$	0.030	$7.87 \pm 0.14$	$-0.119 \pm 0.204$	$-0.0087 \pm 0.0150$	0.087
NGC 2541	$8.45 \pm 0.02$	$-0.608 \pm 0.053$	$-0.0526 \pm 0.0046$	0.030	$0.00 \pm 0.00$	$0.000 \pm 0.000$	$0.0000 \pm 0.0000$	0.000
NGC 2805	$8.51 \pm 0.03$	$-0.432 \pm 0.045$	$-0.0168 \pm 0.0017$	0.040	$7.53 \pm 0.06$	$-0.869 \pm 0.096$	$-0.0338 \pm 0.0037$	0.087
NGC 2835	$8.50 \pm 0.04$	$-0.314 \pm 0.060$	$-0.0324 \pm 0.0062$	0.057	$7.51 \pm 0.10$	$-0.633 \pm 0.149$	$-0.0652 \pm 0.0154$	0.142
NGC 2841	$8.99 \pm 0.08$	$-0.607 \pm 0.172$	$-0.0363 \pm 0.0103$	0.022	$8.81 \pm 0.20$	$-1.488 \pm 0.450$	$-0.0890 \pm 0.0269$	0.052
NGC 2903	$8.82 \pm 0.03$	$-0.523 \pm 0.072$	$-0.0321 \pm 0.0044$	0.061	$8.51 \pm 0.06$	$-1.588 \pm 0.152$	$-0.0975 \pm 0.0093$	0.121
NGC 2997	$8.80 \pm 0.06$	$-0.502 \pm 0.121$	$-0.0318 \pm 0.0076$	0.060	$8.44 \pm 0.13$	$-1.503 \pm 0.274$	$-0.0950 \pm 0.0173$	0.129
NGC 3020	$8.39 \pm 0.02$	$-0.558 \pm 0.041$	$-0.0554 \pm 0.0041$	0.011	$7.27 \pm 0.07$	$-1.053 \pm 0.167$	$-0.1045 \pm 0.0167$	0.045
NGC 3023	$8.34 \pm 0.08$	$-0.444 \pm 0.201$	$-0.0361 \pm 0.0163$	0.054	$7.20 \pm 0.14$	$-0.889 \pm 0.372$	$-0.0722 \pm 0.0302$	0.100
NGC 3031	$8.58 \pm 0.02$	$-0.156 \pm 0.045$	$-0.0110 \pm 0.0032$	0.043	$7.84 \pm 0.06$	$-0.464 \pm 0.116$	$-0.0327 \pm 0.0081$	0.110
NGC 3184	$8.66 \pm 0.02$	$-0.176 \pm 0.037$	$-0.0130 \pm 0.0027$	0.066	$7.86 \pm 0.04$	$-0.338 \pm 0.086$	$-0.0249 \pm 0.0063$	0.137
NGC 3198	$8.60 \pm 0.04$	$-0.425 \pm 0.076$	$-0.0237 \pm 0.0042$	0.063	$7.94 \pm 0.11$	$-1.145 \pm 0.317$	$-0.0638 \pm 0.0176$	0.091

Table 2—Continued

Galaxy	$12+\log(\text{O}/\text{H})_{R_0}$	O/H gradient dex $R_{25}^{-1}$	O/H gradient dex $\text{kpc}^{-1}$	$\sigma(\text{O}/\text{H})$ dex	$12+\log(\text{N}/\text{H})_{R_0}$	N/H gradient dex $R_{25}^{-1}$	N/H gradient dex $\text{kpc}^{-1}$	$\sigma(\text{N}/\text{H})$ dex
NGC 3227	$8.64 \pm 0.05$	$-0.254 \pm 0.077$	$-0.0158 \pm 0.0048$	0.056	$0.00 \pm 0.00$	$0.000 \pm 0.000$	$0.0000 \pm 0.0000$	0.000
NGC 3239	$8.12 \pm 0.01$	$-0.153 \pm 0.012$	$-0.0260 \pm 0.0021$	0.005	$6.78 \pm 0.04$	$-0.275 \pm 0.064$	$-0.0467 \pm 0.0108$	0.026
NGC 3310	$8.37 \pm 0.01$	$-0.101 \pm 0.023$	$-0.0117 \pm 0.0027$	0.040	$7.27 \pm 0.02$	$-0.254 \pm 0.060$	$-0.0295 \pm 0.0070$	0.104
NGC 3319	$8.50 \pm 0.02$	$-0.516 \pm 0.043$	$-0.0408 \pm 0.0034$	0.024	$0.00 \pm 0.00$	$0.000 \pm 0.000$	$0.0000 \pm 0.0000$	0.000
NGC 3344	$8.72 \pm 0.02$	$-0.618 \pm 0.039$	$-0.0984 \pm 0.0063$	0.029	$8.08 \pm 0.17$	$-1.413 \pm 0.252$	$-0.2254 \pm 0.0407$	0.044
NGC 3351	$8.82 \pm 0.01$	$-0.210 \pm 0.031$	$-0.0186 \pm 0.0027$	0.038	$8.51 \pm 0.03$	$-0.678 \pm 0.094$	$-0.0599 \pm 0.0083$	0.116
NGC 3359	$8.40 \pm 0.06$	$-0.271 \pm 0.108$	$-0.0179 \pm 0.0071$	0.099	$7.43 \pm 0.09$	$-0.688 \pm 0.154$	$-0.0453 \pm 0.0102$	0.130
NGC 3486	$8.60 \pm 0.02$	$-0.421 \pm 0.043$	$-0.0447 \pm 0.0046$	0.018	$7.80 \pm 0.04$	$-0.928 \pm 0.088$	$-0.0985 \pm 0.0094$	0.036
NGC 3521	$8.83 \pm 0.04$	$-0.666 \pm 0.096$	$-0.0390 \pm 0.0056$	0.048	$0.00 \pm 0.00$	$0.000 \pm 0.000$	$0.0000 \pm 0.0000$	0.000
NGC 3621	$8.68 \pm 0.02$	$-0.460 \pm 0.035$	$-0.0446 \pm 0.0034$	0.050	$8.05 \pm 0.05$	$-1.298 \pm 0.095$	$-0.1260 \pm 0.0092$	0.133
NGC 3631	$8.71 \pm 0.03$	$-0.414 \pm 0.077$	$-0.0256 \pm 0.0048$	0.024	$7.94 \pm 0.05$	$-0.719 \pm 0.145$	$-0.0445 \pm 0.0090$	0.046
NGC 3718	$8.60 \pm 0.19$	$-0.221 \pm 0.253$	$-0.0119 \pm 0.0136$	0.066	$0.00 \pm 0.00$	$0.000 \pm 0.000$	$0.0000 \pm 0.0000$	0.000
NGC 3820	$8.64 \pm 0.01$	$-0.102 \pm 0.019$	$-0.0116 \pm 0.0022$	0.019	$7.92 \pm 0.05$	$-0.342 \pm 0.093$	$-0.0389 \pm 0.0105$	0.092
NGC 3893	$8.73 \pm 0.16$	$-0.437 \pm 0.254$	$-0.0371 \pm 0.0215$	0.028	$0.00 \pm 0.00$	$0.000 \pm 0.000$	$0.0000 \pm 0.0000$	0.000
NGC 3938	$8.79 \pm 0.05$	$-0.577 \pm 0.092$	$-0.0413 \pm 0.0066$	0.031	$8.15 \pm 0.07$	$-1.204 \pm 0.141$	$-0.0861 \pm 0.0101$	0.048
NGC 4030	$8.77 \pm 0.02$	$-0.258 \pm 0.036$	$-0.0156 \pm 0.0022$	0.010	$8.05 \pm 0.08$	$-0.344 \pm 0.177$	$-0.0208 \pm 0.0107$	0.052
NGC 4088	$8.71 \pm 0.04$	$-0.366 \pm 0.093$	$-0.0305 \pm 0.0078$	0.025	$7.97 \pm 0.06$	$-0.698 \pm 0.116$	$-0.0582 \pm 0.0097$	0.032
NGC 4109	$8.63 \pm 0.03$	$-0.402 \pm 0.099$	$-0.0269 \pm 0.0066$	0.056	$7.87 \pm 0.05$	$-1.152 \pm 0.154$	$-0.0770 \pm 0.0103$	0.081
NGC 4254	$8.77 \pm 0.02$	$-0.353 \pm 0.034$	$-0.0316 \pm 0.0031$	0.036	$8.09 \pm 0.05$	$-0.716 \pm 0.100$	$-0.0641 \pm 0.0090$	0.106
NGC 4258	$8.54 \pm 0.03$	$-0.161 \pm 0.073$	$-0.0083 \pm 0.0037$	0.031	$7.59 \pm 0.13$	$-0.232 \pm 0.282$	$-0.0119 \pm 0.0144$	0.120
NGC 4303	$8.78 \pm 0.03$	$-0.577 \pm 0.073$	$-0.0452 \pm 0.0057$	0.062	$8.24 \pm 0.08$	$-1.370 \pm 0.189$	$-0.1073 \pm 0.0148$	0.156
NGC 4321	$8.74 \pm 0.03$	$-0.219 \pm 0.048$	$-0.0118 \pm 0.0026$	0.038	$8.04 \pm 0.06$	$-0.355 \pm 0.104$	$-0.0192 \pm 0.0056$	0.083

Table 2—Continued

Galaxy	$12+\log(\text{O}/\text{H})_{R_0}$	O/H gradient dex $R_{25}^{-1}$	O/H gradient dex $\text{kpc}^{-1}$	$\sigma(\text{O}/\text{H})$ dex	$12+\log(\text{N}/\text{H})_{R_0}$	N/H gradient dex $R_{25}^{-1}$	N/H gradient dex $\text{kpc}^{-1}$	$\sigma(\text{N}/\text{H})$ dex
NGC 4395	$8.19 \pm 0.05$	$-0.164 \pm 0.082$	$-0.0200 \pm 0.0100$	0.079	$6.89 \pm 0.08$	$-0.346 \pm 0.143$	$-0.0420 \pm 0.0174$	0.136
NGC 4490	$8.29 \pm 0.08$	$-0.318 \pm 0.254$	$-0.0444 \pm 0.0355$	0.058	$7.09 \pm 0.15$	$-0.560 \pm 0.449$	$-0.0781 \pm 0.0629$	0.102
NGC 4501	$8.92 \pm 0.12$	$-0.424 \pm 0.242$	$-0.0299 \pm 0.0171$	0.054	$0.00 \pm 0.00$	$0.000 \pm 0.000$	$0.0000 \pm 0.0000$	0.000
NGC 4535	$8.71 \pm 0.03$	$-0.299 \pm 0.064$	$-0.0163 \pm 0.0035$	0.025	$7.97 \pm 0.03$	$-0.594 \pm 0.055$	$-0.0324 \pm 0.0030$	0.022
NGC 4559	$8.53 \pm 0.03$	$-0.573 \pm 0.056$	$-0.0467 \pm 0.0046$	0.047	$0.00 \pm 0.00$	$0.000 \pm 0.000$	$0.0000 \pm 0.0000$	0.000
NGC 4625	$8.58 \pm 0.01$	$-0.130 \pm 0.044$	$-0.0443 \pm 0.0151$	0.042	$7.84 \pm 0.05$	$-0.680 \pm 0.143$	$-0.2318 \pm 0.0488$	0.127
NGC 4631	$8.39 \pm 0.06$	$-0.333 \pm 0.125$	$-0.0194 \pm 0.0073$	0.077	$7.18 \pm 0.09$	$-0.480 \pm 0.169$	$-0.0280 \pm 0.0098$	0.093
NGC 4651	$8.68 \pm 0.04$	$-0.469 \pm 0.096$	$-0.0343 \pm 0.0070$	0.049	$8.02 \pm 0.10$	$-1.133 \pm 0.233$	$-0.0829 \pm 0.0170$	0.119
NGC 4654	$8.66 \pm 0.04$	$-0.364 \pm 0.083$	$-0.0318 \pm 0.0073$	0.044	$7.90 \pm 0.11$	$-0.797 \pm 0.229$	$-0.0695 \pm 0.0200$	0.120
NGC 4656	$8.06 \pm 0.16$	$-0.551 \pm 0.280$	$-0.0305 \pm 0.0155$	0.084	$6.62 \pm 0.24$	$-0.634 \pm 0.409$	$-0.0351 \pm 0.0227$	0.123
NGC 4713	$8.53 \pm 0.09$	$-0.771 \pm 0.250$	$-0.1325 \pm 0.0428$	0.095	$7.60 \pm 0.14$	$-1.548 \pm 0.397$	$-0.2662 \pm 0.0679$	0.150
NGC 4725	$8.83 \pm 0.37$	$-0.472 \pm 0.853$	$-0.0223 \pm 0.0404$	0.070	$0.00 \pm 0.00$	$0.000 \pm 0.000$	$0.0000 \pm 0.0000$	0.000
NGC 4736	$8.57 \pm 0.03$	$-0.066 \pm 0.170$	$-0.0086 \pm 0.0224$	0.065	$0.00 \pm 0.00$	$0.000 \pm 0.000$	$0.0000 \pm 0.0000$	0.000
NGC 4861	$8.00 \pm 0.06$	$-0.013 \pm 0.092$	$-0.0030 \pm 0.0210$	0.090	$6.54 \pm 0.13$	$-0.058 \pm 0.200$	$-0.0132 \pm 0.0454$	0.193
NGC 5033	$8.64 \pm 0.06$	$-0.278 \pm 0.094$	$-0.0095 \pm 0.0032$	0.090	$8.00 \pm 0.10$	$-0.599 \pm 0.130$	$-0.0206 \pm 0.0045$	0.072
NGC 5055	$8.87 \pm 0.02$	$-0.490 \pm 0.031$	$-0.0337 \pm 0.0021$	0.007	$8.42 \pm 0.10$	$-1.259 \pm 0.186$	$-0.0867 \pm 0.0129$	0.044
NGC 5068	$8.57 \pm 0.04$	$-0.355 \pm 0.098$	$-0.0626 \pm 0.0173$	0.050	$7.53 \pm 0.11$	$-0.451 \pm 0.263$	$-0.0794 \pm 0.0463$	0.134
NGC 5194	$8.88 \pm 0.03$	$-0.324 \pm 0.053$	$-0.0223 \pm 0.0037$	0.062	$8.52 \pm 0.05$	$-0.704 \pm 0.102$	$-0.0484 \pm 0.0070$	0.117
NGC 5236	$8.78 \pm 0.01$	$-0.221 \pm 0.028$	$-0.0256 \pm 0.0032$	0.050	$8.34 \pm 0.03$	$-0.649 \pm 0.058$	$-0.0752 \pm 0.0068$	0.104
NGC 5248	$8.64 \pm 0.03$	$-0.142 \pm 0.076$	$-0.0069 \pm 0.0037$	0.072	$7.74 \pm 0.05$	$-0.132 \pm 0.155$	$-0.0064 \pm 0.0075$	0.146
NGC 5457	$8.71 \pm 0.01$	$-0.840 \pm 0.029$	$-0.0293 \pm 0.0010$	0.076	$8.01 \pm 0.03$	$-1.760 \pm 0.056$	$-0.0613 \pm 0.0020$	0.142
NGC 5474	$8.19 \pm 0.02$	$-0.008 \pm 0.086$	$-0.0019 \pm 0.0182$	0.100	$6.82 \pm 0.03$	$-0.261 \pm 0.144$	$-0.0553 \pm 0.0303$	0.156

Table 2—Continued

Galaxy	$12+\log(\text{O}/\text{H})_{R_0}$	O/H gradient dex $R_{25}^{-1}$	O/H gradient dex $\text{kpc}^{-1}$	$\sigma(\text{O}/\text{H})$ dex	$12+\log(\text{N}/\text{H})_{R_0}$	N/H gradient dex $R_{25}^{-1}$	N/H gradient dex $\text{kpc}^{-1}$	$\sigma(\text{N}/\text{H})$ dex
NGC 5668	$8.52 \pm 0.03$	$-0.471 \pm 0.061$	$-0.0364 \pm 0.0047$	0.075	$7.48 \pm 0.05$	$-1.032 \pm 0.127$	$-0.0796 \pm 0.0098$	0.147
NGC 6384	$8.87 \pm 0.04$	$-0.531 \pm 0.068$	$-0.0228 \pm 0.0029$	0.029	$8.41 \pm 0.12$	$-1.172 \pm 0.197$	$-0.0504 \pm 0.0084$	0.083
NGC 6691	$8.66 \pm 0.02$	$-0.152 \pm 0.052$	$-0.0077 \pm 0.0026$	0.050	$7.98 \pm 0.06$	$-0.414 \pm 0.157$	$-0.0211 \pm 0.0080$	0.142
NGC 6744	$8.88 \pm 0.03$	$-0.726 \pm 0.060$	$-0.0266 \pm 0.0022$	0.034	$8.66 \pm 0.07$	$-1.996 \pm 0.157$	$-0.0731 \pm 0.0057$	0.087
NGC 6946	$8.72 \pm 0.06$	$-0.337 \pm 0.099$	$-0.0337 \pm 0.0099$	0.061	$8.05 \pm 0.15$	$-0.751 \pm 0.237$	$-0.0751 \pm 0.0237$	0.148
NGC 7331	$8.67 \pm 0.08$	$-0.222 \pm 0.193$	$-0.0097 \pm 0.0084$	0.044	$7.75 \pm 0.09$	$-0.056 \pm 0.213$	$-0.0024 \pm 0.0092$	0.048
NGC 7495	$8.61 \pm 0.01$	$-0.260 \pm 0.027$	$-0.0140 \pm 0.0015$	0.028	$7.83 \pm 0.02$	$-0.616 \pm 0.062$	$-0.0333 \pm 0.0033$	0.064
NGC 7518	$8.74 \pm 0.02$	$-0.127 \pm 0.045$	$-0.0122 \pm 0.0043$	0.034	$8.30 \pm 0.07$	$-0.514 \pm 0.136$	$-0.0496 \pm 0.0131$	0.104
NGC 7529	$8.64 \pm 0.04$	$-0.232 \pm 0.067$	$-0.0303 \pm 0.0087$	0.040	$7.97 \pm 0.13$	$-0.752 \pm 0.223$	$-0.0979 \pm 0.0290$	0.133
NGC 7570	$8.58 \pm 0.03$	$-0.086 \pm 0.045$	$-0.0217 \pm 0.0114$	0.029	$7.78 \pm 0.06$	$-0.219 \pm 0.106$	$-0.0549 \pm 0.0265$	0.068
NGC 7591	$8.71 \pm 0.01$	$-0.146 \pm 0.029$	$-0.0085 \pm 0.0017$	0.024	$8.13 \pm 0.06$	$-0.400 \pm 0.114$	$-0.0234 \pm 0.0066$	0.093
NGC 7678	$8.55 \pm 0.04$	$-0.079 \pm 0.078$	$-0.0048 \pm 0.0047$	0.030	$7.64 \pm 0.14$	$-0.081 \pm 0.248$	$-0.0049 \pm 0.0149$	0.094
NGC 7793	$8.50 \pm 0.02$	$-0.305 \pm 0.048$	$-0.0662 \pm 0.0104$	0.071	$7.52 \pm 0.05$	$-0.752 \pm 0.095$	$-0.1631 \pm 0.0207$	0.135
IC 0010	$8.14 \pm 0.08$	$0.252 \pm 0.185$	$0.4294 \pm 0.3025$	0.094	$6.90 \pm 0.15$	$0.355 \pm 0.338$	$0.6035 \pm 0.5534$	0.165
IC 0193	$8.59 \pm 0.02$	$-0.139 \pm 0.064$	$-0.0083 \pm 0.0039$	0.039	$7.80 \pm 0.05$	$-0.306 \pm 0.151$	$-0.0183 \pm 0.0090$	0.092
IC 0208	$8.58 \pm 0.01$	$-0.168 \pm 0.035$	$-0.0165 \pm 0.0034$	0.036	$7.78 \pm 0.03$	$-0.422 \pm 0.083$	$-0.0416 \pm 0.0082$	0.086
IC 0342	$8.83 \pm 0.04$	$-0.513 \pm 0.087$	$-0.0500 \pm 0.0085$	0.045	$8.46 \pm 0.07$	$-1.465 \pm 0.131$	$-0.1426 \pm 0.0128$	0.068
IC 1132	$8.65 \pm 0.03$	$-0.390 \pm 0.059$	$-0.0323 \pm 0.0049$	0.077	$7.69 \pm 0.06$	$-0.598 \pm 0.106$	$-0.0495 \pm 0.0087$	0.128
IC 2204	$8.62 \pm 0.01$	$-0.160 \pm 0.033$	$-0.0159 \pm 0.0033$	0.024	$7.89 \pm 0.03$	$-0.387 \pm 0.086$	$-0.0384 \pm 0.0086$	0.064
IC 5201	$8.35 \pm 0.07$	$-0.501 \pm 0.147$	$-0.0316 \pm 0.0093$	0.074	$7.19 \pm 0.12$	$-0.908 \pm 0.242$	$-0.0573 \pm 0.0153$	0.122
IC 5309	$8.70 \pm 0.03$	$-0.058 \pm 0.066$	$-0.0059 \pm 0.0067$	0.059	$8.08 \pm 0.09$	$-0.211 \pm 0.206$	$-0.0215 \pm 0.0210$	0.170
UGC 00223	$8.53 \pm 0.02$	$-0.099 \pm 0.053$	$-0.0105 \pm 0.0057$	0.029	$7.72 \pm 0.06$	$-0.295 \pm 0.152$	$-0.0313 \pm 0.0162$	0.084

Table 2—Continued

Galaxy	$12+\log(\text{O}/\text{H})_{R_0}$	O/H gradient dex $R_{25}^{-1}$	O/H gradient dex $\text{kpc}^{-1}$	$\sigma(\text{O}/\text{H})$ dex	$12+\log(\text{N}/\text{H})_{R_0}$	N/H gradient dex $R_{25}^{-1}$	N/H gradient dex $\text{kpc}^{-1}$	$\sigma(\text{N}/\text{H})$ dex
UGC 01087	$8.60 \pm 0.01$	$-0.246 \pm 0.023$	$-0.0192 \pm 0.0018$	0.026	$7.83 \pm 0.03$	$-0.609 \pm 0.058$	$-0.0475 \pm 0.0045$	0.066
UGC 01862	$8.43 \pm 0.02$	$-0.094 \pm 0.039$	$-0.0194 \pm 0.0081$	0.040	$7.42 \pm 0.04$	$-0.316 \pm 0.090$	$-0.0651 \pm 0.0186$	0.092
UGC 02023	$8.13 \pm 0.19$	$-0.088 \pm 0.280$	$-0.0358 \pm 0.1128$	0.075	$6.84 \pm 0.29$	$-0.197 \pm 0.434$	$-0.0800 \pm 0.1752$	0.115
UGC 02216	$8.08 \pm 0.02$	$-0.068 \pm 0.052$	$-0.0099 \pm 0.0077$	0.024	$6.72 \pm 0.04$	$-0.124 \pm 0.094$	$-0.0181 \pm 0.0137$	0.041
UGC 02345	$8.04 \pm 0.03$	$-0.893 \pm 0.085$	$-0.0885 \pm 0.0084$	0.041	$6.63 \pm 0.11$	$-0.846 \pm 0.255$	$-0.0838 \pm 0.0253$	0.131
UGC 03701	$8.41 \pm 0.01$	$-0.087 \pm 0.046$	$-0.0076 \pm 0.0040$	0.042	$7.41 \pm 0.03$	$-0.329 \pm 0.102$	$-0.0288 \pm 0.0089$	0.092
UGC 04107	$8.56 \pm 0.01$	$-0.231 \pm 0.041$	$-0.0219 \pm 0.0039$	0.045	$7.72 \pm 0.03$	$-0.498 \pm 0.087$	$-0.0470 \pm 0.0083$	0.096
UGC 04305	$7.89 \pm 0.07$	$-0.225 \pm 0.137$	$-0.0573 \pm 0.0352$	0.075	$6.41 \pm 0.13$	$-0.307 \pm 0.246$	$-0.0784 \pm 0.0629$	0.139
UGC 05100	$8.58 \pm 0.05$	$-0.078 \pm 0.075$	$-0.0056 \pm 0.0053$	0.047	$7.90 \pm 0.13$	$-0.220 \pm 0.204$	$-0.0156 \pm 0.0145$	0.119
UGC 06410	$8.58 \pm 0.02$	$-0.148 \pm 0.040$	$-0.0113 \pm 0.0031$	0.057	$7.78 \pm 0.05$	$-0.454 \pm 0.093$	$-0.0345 \pm 0.0071$	0.123
UGC 08091	$7.58 \pm 0.04$	$0.177 \pm 0.067$	$0.5487 \pm 0.2003$	0.055	$6.03 \pm 0.08$	$0.255 \pm 0.129$	$0.7891 \pm 0.3905$	0.108
UGC 09562	$8.22 \pm 0.05$	$-0.193 \pm 0.143$	$-0.0585 \pm 0.0433$	0.080	$6.80 \pm 0.06$	$-0.206 \pm 0.144$	$-0.0626 \pm 0.0437$	0.068
UGC 09837	$8.45 \pm 0.02$	$-0.412 \pm 0.076$	$-0.0370 \pm 0.0068$	0.078	$7.32 \pm 0.04$	$-0.820 \pm 0.140$	$-0.0738 \pm 0.0126$	0.141
UGC 10445	$8.27 \pm 0.04$	$-0.082 \pm 0.077$	$-0.0103 \pm 0.0096$	0.050	$7.03 \pm 0.08$	$-0.197 \pm 0.141$	$-0.0246 \pm 0.0176$	0.091
UGC 12709	$8.47 \pm 0.08$	$-0.706 \pm 0.218$	$-0.0434 \pm 0.0134$	0.082	$7.30 \pm 0.15$	$-1.089 \pm 0.418$	$-0.0669 \pm 0.0257$	0.157
PGC 29167	$8.34 \pm 0.10$	$0.152 \pm 0.169$	$0.0507 \pm 0.0565$	0.040	$7.25 \pm 0.01$	$0.005 \pm 0.020$	$0.0017 \pm 0.0065$	0.005
PGC 41318	$8.45 \pm 0.04$	$-0.168 \pm 0.143$	$-0.0281 \pm 0.0239$	0.033	$7.28 \pm 0.17$	$-0.563 \pm 0.568$	$-0.0941 \pm 0.0945$	0.130
PGC 44772	$8.59 \pm 0.03$	$-0.268 \pm 0.045$	$-0.0216 \pm 0.0036$	0.043	$7.79 \pm 0.07$	$-0.705 \pm 0.115$	$-0.0569 \pm 0.0093$	0.109
PGC 45195	$8.14 \pm 0.04$	$-0.152 \pm 0.059$	$-0.0122 \pm 0.0047$	0.035	$6.81 \pm 0.08$	$-0.277 \pm 0.104$	$-0.0223 \pm 0.0084$	0.061
PGC 46182	$8.59 \pm 0.03$	$-0.126 \pm 0.078$	$-0.0089 \pm 0.0055$	0.035	$7.92 \pm 0.11$	$-0.462 \pm 0.313$	$-0.0327 \pm 0.0221$	0.141



Table 3. List of references for the emission line flux measurements in the extragalactic H II regions.

Galaxy	Reference
NGC 0012	Sánchez et al. (2012)
NGC 0055	Webster & Smith (1983), Stasińska et al. (1986), Tüllmann et al. (2003)
NGC 0099	Sánchez et al. (2012), SDSS
NGC 0224 (M 31)	Dennefeld & Kunth (1981), Blair et al. (1982), Galarza et al. (1999), Bresolin et al. (1999), Esteban et al. (2009), Zurita & Bresolin (2012), Sanders et al. (2012)
NGC 0234	Sánchez et al. (2012), SDSS
NGC 0253	Webster & Smith (1983)
NGC 0300	Pagel et al. (1979), Webster & Smith (1983), Edmunds & Pagel (1984), Bresolin et al. (2009a)
NGC 0428	SDSS
NGC 0450	Fernandes et al. (2004), SDSS
NGC 0493	SDSS
NGC 0575	Sánchez et al. (2012)
NGC 0598 (M 33)	Smith (1975), Kwitter & Aller (1981), McCall et al. (1985), Díaz et al. (1987), Vílchez et al. (1988b), Bresolin et al. (1999), Jamet et al. (2005), Esteban et al. (2009), Bresolin et al. (2010), Magrini et al. (2010), Relaño et al. (2010), Kehrig et al. (2011)
NGC 0628 (M 74)	McCall et al. (1985), Ferguson et al. (1998), van Zee et al. (1998), Bresolin et al. (1999), Rosales-Ortega et al. (2011), Gusev et al. (2012)
NGC 0753	Henry et al. (1996)
NGC 0783	Gusev et al. (2012)
NGC 0925	van Zee et al. (1998)
NGC 1055	SDSS
NGC 1058	Ferguson et al. (1998), Sánchez et al. (2012)
NGC 1068 (M 77)	Evans & Dopita (1987), Oey & Kennicutt (1993), van Zee et al. (1998), SDSS

Table 3—Continued

Galaxy	Reference
NGC 1090	SDSS
NGC 1097	Phillips et al. (1984), Storch-Bergmann et al. (1996b)
NGC 1232	van Zee et al. (1998), Bresolin et al. (2005)
NGC 1313	Pagel et al. (1980), Walsh & Roy (1997), Hadfield & Crowther (2007)
NGC 1365	Pagel et al. (1979), Alloin et al. (1981), Roy & Walsh (1997), Bresolin et al. (2005)
NGC 1512	Bresolin et al. (2012)
NGC 1598	Storch-Bergmann et al. (1996a)
NGC 1637	van Zee et al. (1998), Sánchez et al. (2012)
NGC 1642	Sánchez et al. (2012)
NGC 1672	Storch-Bergmann et al. (1996b)
NGC 2336	Gusev et al. (2012)
NGC 2403	Smith (1975), McCall et al. (1985), Fierro et al. (1986), Garnett et al. (1997), van Zee et al. (1998), Bresolin et al. (1999), Garnett et al. (1999), Esteban et al. (2009), SDSS
NGC 2441	Sánchez et al. (2012)
NGC 2442	Ryder (1995)
NGC 2541	Zaritsky et al. (1994), SDSS
NGC 2805	van Zee et al. (1998), SDSS
NGC 2835	Ryder (1995)
NGC 2841	Oey & Kennicutt (1993), Bresolin et al. (1999)
NGC 2903	McCall et al. (1985), Bresolin et al. (2005), Díaz et al. (2007), SDSS
NGC 2997	Edmunds & Pagel (1984), Firpo et al. (2005), Bresolin et al. (2005)
NGC 3020	SDSS
NGC 3023	SDSS



Table 3—Continued

Galaxy	Reference
NGC 3031 (M 81)	Stauffer & Bothun (1984), Garnett & Shields (1987), Bresolin et al. (1999), Staghellini et al. (2010), Patterson et al. (2012), SDSS
NGC 3184	McCall et al. (1985), van Zee et al. (1998), Sánchez et al. (2012), SDSS
NGC 3198	Zaritsky et al. (1994), SDSS
NGC 3227	González Delgado & Pérez (1997), Lisenfeld et al. (2008), Werk et al. (2011)
NGC 3239	SDSS
NGC 3310	Bresolin et al. (1999), Sánchez et al. (2012)
NGC 3319	Zaritsky et al. (1994), SDSS
NGC 3344	McCall et al. (1985), Vílchez et al. (1988a), Zaritsky et al. (1994), SDSS
NGC 3351 (M 95)	McCall et al. (1985), Bresolin et al. (1999), Bresolin & Kennicutt (2002), Díaz et al. (2007), SDSS
NGC 3359	Zahid & Bresolin (2011), SDSS
NGC 3486	SDSS
NGC 3521	Bresolin et al. (1999), Zaritsky et al. (1994)
NGC 3621	Ryder (1995), Bresolin et al. (2012)
NGC 3631	SDSS
NGC 3718	Werk et al. (2011)
NGC 3820	Sánchez et al. (2012), SDSS
NGC 3893	Werk et al. (2011)
NGC 3938	SDSS
NGC 4030	SDSS
NGC 4088	SDSS
NGC 4109	Sánchez et al. (2012)
NGC 4254 (M 99)	McCall et al. (1985), Shields et al. (1991), Henry et al. (1994), SDSS

Table 3—Continued

Galaxy	Reference
NGC 4258 (M 106)	Bresolin et al. (1999), Díaz et al. (2000), SDSS
NGC 4303 (M 61)	Shields et al. (1991), Henry et al. (1994), SDSS
NGC 4321 (M 100)	McCall et al. (1985), Shields et al. (1991), SDSS
NGC 4395	McCall et al. (1985), van Zee et al. (1998), Esteban et al. (2009), SDSS
NGC 4490	SDSS
NGC 4501	Skillman et al. (1996)
NGC 4535	SDSS
NGC 4559	Zaritsky et al. (1994), SDSS
NGC 4625	Goddard et al. (2011), Bresolin et al. (2009b), SDSS
NGC 4631	Roy et al. (1991), SDSS
NGC 4651	Skillman et al. (1996), SDSS
NGC 4654	Skillman et al. (1996), SDSS
NGC 4656	SDSS
NGC 4713	Skillman et al. (1996), SDSS
NGC 4725	Zaritsky et al. (1994)
NGC 4736 (M 94)	Bresolin et al. (1999), Oey & Kennicutt (1993), Rodrigues et al. (1998)
NGC 4861	Dinerstein & Shields (1986), Kobulnicky & Skillman (1998), Izotov et al. (1997), Bresolin et al. (1999), Noeske et al. (2000), Esteban et al. (2009), SDSS
NGC 5033	Zaritsky et al. (1994), SDSS
NGC 5055 (M 63)	McCall et al. (1985)
NGC 5068	Ryder (1995)
NGC 5194 (M 51)	McCall et al. (1985), Díaz et al. (1991), Bresolin et al. (1999), Garnett et al. (2004), SDSS, Bresolin et al. (2004)

Table 3—Continued

Galaxy	Reference
NGC 5236 (M 83)	Dufour et al. (1980), Bresolin et al. (1999), Bresolin & Kennicutt (2002), Bresolin et al. (2005), Esteban et al. (2009), Bresolin et al. (2009b)
NGC 5248	Storchi-Bergmann et al. (1996b), SDSS
NGC 5457 (M 101)	Smith (1975), Hawley (1978), Sedwick & Aller (1981), Rayo et al. (1982), Skillman (1985), McCall et al. (1985), Torres-Peimbert et al. (1989), Kinkel & Rosa (1994), Garnett & Kennicutt (1994), Kennicutt & Garnett (1996), SDSS, van Zee et al. (1998), Luridiana et al. (2002), Kennicutt et al. (2003), Bresolin (2007), Izotov et al. (2007), Esteban et al. (2009)
NGC 5474	Sánchez et al. (2012), SDSS
NGC 5668	Marino et al. (2012), SDSS
NGC 6384	Bresolin et al. (1999), Bresolin & Kennicutt (2002)
NGC 6691	Sánchez et al. (2012)
NGC 6744	Ryder (1995)
NGC 6946	McCall et al. (1985), Ferguson et al. (1998), García-Benito et al. (2010)
NGC 7331	Bresolin et al. (1999), Gusev et al. (2012)
NGC 7495	Sánchez et al. (2012)
NGC 7518	Robertson et al. (2012)
NGC 7529	Robertson et al. (2012)
NGC 7570	Sánchez et al. (2012)
NGC 7591	Robertson et al. (2012)
NGC 7678	Gusev et al. (2012)
NGC 7793	Webster & Smith (1983), Edmunds & Pagel (1984), McCall et al. (1985), Bibby & Crowther (2010)
IC 0010	Lequeux et al. (1979), Richer et al. (2001), Magrini & Gonçalves (2009)
IC 0193	Sánchez et al. (2012)

Table 3—Continued

Galaxy	Reference
IC 0208	Sánchez et al. (2012)
IC 0342	McCall et al. (1985)
IC 1132	Sánchez et al. (2012)
IC 2204	Sánchez et al. (2012), SDSS
IC 5201	Ryder (1995)
IC 5309	Robertson et al. (2012)
UGC 00223	Sánchez et al. (2012), SDSS
UGC 01087	Sánchez et al. (2012)
UGC 01862	Sánchez et al. (2012)
UGC 02023	van Zee & Haynes (2006)
UGC 02216	SDSS
UGC 02345	SDSS
UGC 03701	Sánchez et al. (2012)
UGC 04107	Sánchez et al. (2012), SDSS
UGC 04305	Croxall et al. (2009)
UGC 05100	Sánchez et al. (2012)
UGC 06410	Sánchez et al. (2012), SDSS
UGC 08091 (GR 8)	Moles et al. (1990), van Zee et al. (2006), SDSS
UGC 09562	Pérez-Montero et al. (2009), SDSS
UGC 09837	Sánchez et al. (2012), SDSS
UGC 10445	van Zee & Haynes (2006), SDSS
UGC 12709	SDSS
PGC 029167	Croxall et al. (2009)

Table 3—Continued

Galaxy	Reference
PGC 041318	Sánchez et al. (2012)
PGC 044772	Sánchez et al. (2012)
PGC 045195	SDSS
PGC 046182	SDSS, Sánchez et al. (2012)